Four-Wave Mixing in Semiconductor Optical Amplifiers for Terahertz Spectroscopy and Wavelength Conversion

Thesis by

Jianhui Zhou

In Partial Fulfillment of the Requirements

for the Degree of

Doctor of Philosophy

California Institute of Technology

Pasadena, California

1995

(Defended May 11, 1995)

To My Wife, Xiaoyu

Acknowledgments

First and foremost, I wish to express deep thanks to my advisor, Professor Kerry Vahala. I have thoroughly enjoyed working with him and learning from him. His keen physical insight has continually provided invaluable guidance. His dedication and enthusiasm has set an example for me of how to do science, and any professional work. I will always look back with pride on what I have accomplished with him at Caltech in the past five years.

Some of the measurements in this thesis were performed using Erbium-doped fiber ring lasers developed by Dr. Namkyoo Park and Dr. Jay Dawson, then graduate students in the group, to whom I owe special thanks. Thanks are also due to David Geraghty for his collaboration on the wavelength conversion system measurement. I would also like to thank other members, present and past, in the Vahala group who have shared with me many stimulating discussions and have helped make my Ph.D. pursuit an enjoyable and rewarding experience: Robert Lee, Roberto Paiella, Guido Hunziker, Charles Tsai, Minyu Yao, Masashi Fukazawa, Hunsuk Kim, Renato Camata, Dr. John Lebens, Dr. Winston Saunders, Dr. Pete Sercel, and Dr. Steve Sanders. The assistance of Rosalie Rowe on day to day matters is much appreciated.

The semiconductor optical amplifiers used in the measurements were supplied by AT&T Bell Laboratories. Special thanks are due to Drs. Michael Newkirk, Barry Miller and Tom Koch who have donated their time and expertise. Michael has also made valuable comments at the early stage of this thesis research. Ortel Corporation has donated some of the DFB lasers and photodetectors used in the experiments

described in this thesis. In addition, the Advanced Research Projects Agency, the Office of Naval Research and the National Science Foundation provided funding for much of the research in this thesis.

My growth as an independent scientist in the past five years has also benefited greatly from interactions with scientists and researchers outside Caltech. In particular, my appreciation goes to Dr. Tingye Li of AT&T Bell Labs, Dr. Norman Kwong of Ortel, Dr. Antonio Mecozzi of FUB, Italy, Dr. Tien-Pei Lee of Bellcore, Dr. Katie Hall of MIT and Prof. Kam-Yin Lau of UC-Berkeley. I especially thank Dr. Tingye Li who has generously spent his valuable time giving me much appreciated encouragement and advice.

I would also like to thank my parents, brother and sister for their unwavering support throughout the years of my education. Finally, my deepest thanks go to my wife, Xiaoyu. Her understanding, support, encouragement and love during these past five years have been the greatest.

Abstract

Four-wave mixing in semiconductor gain media from GHz to THz detuning rates was used as a frequency-domain technique for analysis of carrier relaxation mechanisms having relaxation times extending from nanosecond to femtosecond time scales. Measurements of four-wave mixing in various semiconductor traveling-wave amplifiers were performed for detuning frequencies as large as 1.7 THz. Ultrafast intraband mechanisms having relaxation time constants of 650 fs, in agreement with dynamic carrier heating, and of less than 100 fs, in agreement with intraband carrier-carrier scattering, were determined in the measurements.

A novel cross-polarized four-wave mixing technique was also developed to study the inter quantum well carrier transport process in quantum well amplifiers. A semiconductor optical amplifier having a structure of alternating tensile and compressively strained quantum wells was used. Polarization selection rule of the strained quantum wells enables selective excitation and probing of adjacent quantum wells according to polarization, thereby enabling study of inter-well carrier transport. A one-dimensional diffusion model was developed to illustrate the different transport efficiencies for carrier number and temperature modulations, thereby qualitatively explaining the experimental data. The inter-well carrier number transport rate in the device measured was determined to be greater than 100 GHz.

Four-wave mixing in semiconductor optical amplifiers was also studied as a wavelength conversion technique. Conversion efficiency over spans up to 65 nm was measured, and wavelength conversion with gain was also demonstrated. It was found

theoretically and confirmed experimentally that the conversion efficiency varies with the cube of the saturated amplifier gain. Noise characteristics of four-wave mixing wavelength converters and their dependence on various device and operational parameters were also studied. Noise reduction by introducing a filter between the preamplifier and the mixer was demonstrated and significant noise reduction was achieved. Finally, wavelength conversion of modulated signals at data rates of 2.5 Gb/s and 10 Gb/s was demonstrated.

Contents

List of Figures

Chapter 1

Introduction

Semiconductor optical amplifiers (SOA's) are of increasing interest for applications in broadband lightwave communication systems such as broadband wavelength conversion and ultrafast optical signal processing [1]. It is interesting to note that most of these applications are not due to the SOA's amplifying nature, but rather due to their nonlinearities. While the linear characteristics of these devices have been well understood, their nonlinear properties are not yet well established.

In this thesis, four-wave mixing experiments in SOA's and accompanying theory are presented which explore intraband dynamics of semiconductor active layers and inter quantum well carrier transport dynamics. Broadband wavelength conversion using four-wave mixing in SOA's is also studied for applications in future multichannel lightwave communication networks. Results concerning conversion efficiency, noise properties, and system impact are presented. The SOA's used in this thesis research are InGaAs/InGaAsP strained multiple quantum well traveling-wave amplifiers operating at 1.5 μm. This is the most important communication band since it is where

silica fibers exhibit minimum attenuation (~ 0.2 dB/km) and where high-performance Erbium-doped fiber amplifiers are available [2].

Chapter 2 is an introduction to semiconductor lasers and amplifiers. It contains basic semiconductor laser physics necessary to understand the four-wave mixing spectroscopy work described in this thesis.

In Chapter 3, the theory governing the four-wave mixing process in SOA's is presented which accounts for contributions to four-wave mixing from both interband and intraband dynamics. Coupled-amplitude equations are solved and an analytical expression for four-wave mixing signal strength is obtained.

Chapter 4 describes four-wave mixing experiments in which four-wave mixing signal spectra are measured at detuning frequencies up to 1.7 THz. Analysis of these signal spectra reveals ultrafast intraband dynamics in agreement with dynamic carrier heating and intraband carrier-carrier scattering processes.

Chapter 5 describes a novel cross-polarized four-wave mixing technique that we developed to study inter quantum well carrier transport. The experimental data are qualitatively explained by noting the different transport efficiencies for carrier number and temperature modulations. In addition, the inter-well carrier number transport rate in the device measured is determined to be greater than 100 GHz.

Chapter 6 first presents an introduction to fiber-optic communications and ongoing efforts for next generation multiwavelength all-optical networks. This review is intended to help explain the application of SOA four-wave mixing wavelength conversion described in this chapter. Results concerning the conversion efficiency over

spans up to 65 nm, as well as a demonstration of wavelength conversion with gain are presented. Issues concerning the noise properties of four-wave mixing wavelength converters are also addressed. Finally, a demonstration of wavelength conversion of modulated signals at data rates of 2.5 Gb/s and 10 Gb/s is described and the experimental results are discussed.

Work presented here is contained in the following published articles and conference proceedings [3]–[21].

Bibliography

[1] S. Shimada, K. Nakagawa, M. Saruwatari, and T. Matsumoto, "Very-high-speed optical signal processing," *Proc. IEEE*, vol. 81, pp. 1633–1646, 1993.

[2] T. Li, "The impact of optical amplifiers on long-distance lightwave telecommunications," *Proc. IEEE*, vol. 81, pp. 1633–1646, 1993.

[3] J. Zhou, N. Park, J. W. Dawson, K. J. Vahala, M. A. Newkirk, U. Koren, and B. I. Miller, "Highly nondegenerate four-wave mixing and gain nonlinearity in a strained multiple-quantum-well optical amplifier," *Appl. Phys. Lett.*, vol. 62, pp. 2301–2303, 1993.

[4] J. Zhou, N. Park, J. W. Dawson, K. J. Vahala, M. A. Newkirk, and B. I. Miller, "Terahertz four-wave mixing spectroscopy for study of ultrafast dynamics in a semiconductor optical amplifier," *Appl. Phys. Lett.*, vol. 63, pp. 1179–1181, 1993.

[5] J. Zhou, N. Park, J. W. Dawson, K. J. Vahala, M. A. Newkirk, and B. I. Miller, "Efficiency of broadband four-wave mixing wavelength conversion using semiconductor traveling-wave amplifiers," *IEEE Photon. Technol. Lett.*, vol. 6, pp. 50–52, 1994.

[6] J. Zhou, N. Park, K. J. Vahala, M. A. Newkirk, and B. I. Miller, "Broadband wavelength conversion with amplification by four-wave mixing in semiconductor traveling-wave amplifiers," *Electron. Lett.*, vol. 30, pp. 859–860, 1994.

[7] J. Zhou, N. Park, K. J. Vahala, M. A. Newkirk, and B. I. Miller, "Four-wave mixing wavelength conversion efficiency in semiconductor traveling-wave amplifiers measured to 65 nm of wavelength shift," *IEEE Photon. Technol. Lett.*, vol. 6, pp. 984–987, 1994.

[8] J. Zhou, N. Park, K. J. Vahala, M. A. Newkirk, and B. I. Miller, "Study of inter-well carrier transport by terahertz four-wave mixing in an optical amplifier with tensile and compressively strained quantum wells," *Appl. Phys. Lett.*, vol. 65, pp. 1897–1899, 1994.

[9] K. J. Vahala, J. Zhou, N. Park, J. W. Dawson, M. A. Newkirk, and B. I. Miller, "Measurement of gain nonlinearity in a strained multiple-quantum-well optical amplifier by highly nondegenerate four-wave mixing," *Conference on Lasers and Electro-Optics*, Baltimore, Maryland, May 2–7, 1993, paper JTHA6.

[10] K. J. Vahala, J. Zhou, N. Park, J. W. Dawson, M. A. Newkirk, and B. I. Miller, "Terahertz four-wave mixing spectroscopy of intraband dynamics in quantum well amplifiers," *Conference on Lasers and Electro-Optics*, Baltimore, Maryland, May 2–7, 1993, paper CPD2.

[11] J. Zhou, N. Park, J. W. Dawson, K. J. Vahala, M. A. Newkirk, and B. I. Miller, "Efficiency of broadband wavelength conversion by four-wave mixing in semiconductor traveling-wave amplifiers," *IEEE Lasers and Electro-Optics Society 1993 Annual Meeting*, San Jose, California, November 15–18, 1993, paper OS3.2.

[12] J. Zhou, N. Park, K. J. Vahala, M. A. Newkirk, and B. I. Miller, "Inter quantum-well carrier transport probed by THz four-wave mixing spectroscopy in a semiconductor optical amplifier," *Conference on Lasers and Electro-Optics*, Anaheim, California, May 8–13, 1994, paper CThF1.

[13] J. Zhou, N. Park, K. J. Vahala, M. A. Newkirk, and B. I. Miller, "Wide-band lossless wavelength conversion by four-wave mixing in semiconductor traveling-wave amplifiers," *Conference on Lasers and Electro-Optics*, Anaheim, California, May 8–13, 1994, paper CThA7.

[14] K. J. Vahala, J. Zhou, N. Park, M. A. Newkirk, and B. I. Miller, "Broadband optical wavelength conversion with gain by four-wave mixing in a semiconductor traveling-wave amplifier," *Conference on Lasers and Electro-Optics*, Anaheim, California, May 8–13, 1994, paper CPD4.

[15] K. J. Vahala, J. Zhou, N. Park, M. A. Newkirk, and B. I. Miller, "Four-wave mixing in semiconductor traveling-wave amplifiers for efficient, broadband, wavelength conversion up to 65 nm," *1994 IEEE Nonlinear Optics Conference*, Waikoloa, Hawaii, July 25–29, 1994, paper TuA2.

[16] J. Zhou, N. Park, K. J. Vahala, M. A. Newkirk, and B. I. Miller, "High efficiency, broadband, wavelength conversion by four-wave mixing in semiconductor traveling-wave amplifiers," *Optical Amplifiers and Their Applications Topical Meeting*, Breckenridge, Colorado, August 3–5, 1994, paper FC3.

[17] J. Zhou, N. Park, K. J. Vahala, M. A. Newkirk, and B. I. Miller, "Efficient, broadband, wavelength conversion by four-wave mixing in semiconductor traveling-wave amplifiers," *Optical Society of America 1994 Annual Meeting*, Dallas, Texas, October 2–7, 1994, paper THOO3.

[18] J. Zhou, N. Park, K. J. Vahala, M. A. Newkirk, and B. I. Miller, "Terahertz four-wave mixing in semiconductor optical amplifiers: physics and applications," *SPIE Photonics West*, San Jose, California, February 6–10, 1995. (**Invited**)

[19] K. J. Vahala, J. Zhou, N. Park, M. A. Newkirk, and B. I. Miller, "Four-wave mixing in semiconductor optical amplifiers for wavelength conversion and terahertz spectroscopy," *Conference on Lasers and Electro-Optics*, Baltimore, Maryland, May 21–26, 1995, paper CThF5. (**Invited**)

[20] J. Zhou and K. J. Vahala, "Spontaneous noise reduction in four-wave mixing wavelength converters," *Conference on Lasers and Electro-Optics*, Baltimore, Maryland, May 21–26, 1995, paper CThT1.

[21] K. J. Vahala, J. Zhou, M. A. Newkirk, and B. I. Miller, "Wavelength shifting by four-wave mixing in semiconductor optical amplifiers," *IEEE Lasers and Electro-Optics Society 1995 Annual Meeting*, San Francisco, California, October 30 – November 2, 1995. (**Invited**)

Chapter 2

Semiconductor Lasers and Amplifiers

2.1 Introduction

Optical amplification and feedback are two essential requirements for lasing oscillation. In semiconductor lasers, amplification is accomplished by an electrically pumped active region sandwiched in the middle of a p-n junction, and in the simplest laser device, *i.e.*, Fabry-Perot laser, feedback is provided by the reflection of the cleaved facets of the laser chip. More sophisticated feedback structures have also been developed for better laser performance, for example, distributed-feedback (DFB) devices are lasers in which optical feedback, as the name implies, is not provided by the localized facet mirrors but by a built-in grating that is distributed throughout the laser cavity.

The semiconductor material systems for laser fabrication are generally of two main

types, the GaAs/GaAlAs system and InP/InGaAsP system. GaAs/GaAlAs devices typically have lasing wavelengths in the range 0.7 – 0.9 μm while InP/InGaAsP devices generally lase at longer wavelengths within the 1.1 – 1.6 μm range. The longer wavelength lasers are important for long-haul optical communication because at these wavelengths silica fibers have extremely low attenuation (as low as 0.2 dB/km at 1.55 μm). Other material systems have been investigated extensively in recent years for laser operation in other regions of the optical spectrum, for example, in the visible spectrum for applications in medical diagnostics, bright displays and high-density optical data storage and also for replacement of bulky and expensive solid and gas lasers.

Laser operation of a semiconductor p-n junction device was first demonstrated by four independent research groups within six weeks of one another in 1962 [1]–[4]. Initially, due to the severe heating problems caused by the high lasing threshold current, lasing action could only be generated continuously at low temperature or in pulsed operation at room temperature, and device lifetimes were also short. Since that time, semiconductor lasers have developed at a remarkable pace [5]–[8]. Fabrication technology and device design have progressed to the point where highly reliable lasers with extrapolated room temperature lifetimes of a century are routinely produced.

Because of their low cost, reliability, low power consumption, and capability for high-speed modulation, among other features, semiconductor lasers are technologically attractive sources of coherent optical radiation for a variety of applications. Most notably, semiconductor lasers are playing an integral part in the ever-expanding

lightwave communication industry. One of the most important characteristics for semiconductor lasers used in lightwave communication systems is the direct modulation bandwidth. Part of this thesis studies two physical mechanisms that can limit semiconductor laser modulation bandwidth: ultrafast intraband dynamics and inter quantum well carrier transport.

When the cleaved facets of a semiconductor laser are anti-reflection coated, the device is referred to as a semiconductor optical amplifier (SOA). Two types of SOA's can be distinguished, Fabry-Perot amplifier and traveling-wave amplifier. The former is essentially a laser biased above transparency but below lasing threshold. The result is an amplifier having a series of narrow bandpasses with the resonant-enhanced gain as the envelope. With the latter, on the other hand, great care is exerted to make the reflectivity of both facets as low as possible, typically as low as $10^{-4} - 10^{-5}$. The device will amplify the incident signal in a single pass through the active region, thus with little cavity-resonance effects in the gain spectrum.

Research on SOA's dates back to the 1960's, soon after the invention of semiconductor lasers [9],[10]. However, it was only during the 1980's that SOA's were developed for practical applications, largely motivated by potential applications in lightwave communication systems [11]–[15]. Early studies were conducted on Fabry-Perot amplifiers [9]–[11], but more recent research has concentrated on traveling-wave amplifiers [16]–[18]. Several ways of suppressing the end reflectivity have been demonstrated to obtain traveling-wave operation. These include multi-layer anti-reflection coating [16], angled facet [17], and window facet structures [18].

SOA's have been used as pre-amplifiers [19] and in-line amplifiers [20] in a number of lightwave transmission system experiments. They have also been employed to overcome distribution losses in the local area network applications [21]. However, SOA's, initially developed for optical amplification, have in recent years largely given up the role in the 1.5 μm communication window to Erbium-doped fiber amplifiers which are far superior as optical amplifiers [22]. SOA's have nevertheless found other "unconventional" applications to which a large body of research has been devoted in recent years [23]–[26]. These efforts include using SOA nonlinearities to achieve important functionalities for lightwave communication systems such as broadband wavelength conversion [23],[24], all optical clock recovery [25] and ultrafast optical signal processing [26]. In addition, SOA's are important components in photonic integrated circuits [27].

In this chapter, optical gain in semiconductors is reviewed. Gain nonlinearities, which are responsible for nonlinear applications of SOA's, and the physical processes associated with these nonlinearities, *i.e.*, dynamic carrier heating and spectral hole burning, are also analyzed.

2.2 Optical Gain in Semiconductors

The wave function of an electron in a given band (conduction or valence) in semiconductors can be written as

$$\Psi_{c,v}(\mathbf{r}) = u_{c,v\mathbf{k}}(\mathbf{r})e^{i\mathbf{k}\cdot\mathbf{r}} \tag{2.1}$$

where the subscripts c and v denote for conduction and valence bands, respectively, and $u_{c,v\mathbf{k}}(\mathbf{r})$ has the periodicity of the crystalline lattice. The "propagation" constant $\mathbf{k}$ is quantized and its components are given by

$$k_j = \frac{2\pi m}{L_j} \tag{2.2}$$

where $j = x, y, z$; m is an integer; and L_j is the length of the crystal in the j direction. The $\mathbf{k}$ space volume for each electronic state is thus $8\pi^3/V$ where V is the crystal's physical volume. The number of electronic states per band for a value of k between k and $k + dk$ is given by

$$\rho(k)dk = \frac{k^2 V}{\pi^2} dk \tag{2.3}$$

where a factor of two has been added accounting for the two spin states of electrons for each k eigenvalue.

Using the parabolic band approximation

$$E(k) = \frac{\hbar^2 k^2}{2m^*} \tag{2.4}$$

where m^* is the effective mass and the energy E is measured from the band edge extremum, the density of states per unit energy interval can be readily expressed as

$$\rho_{c,v}(E) = \frac{1}{V}\rho_{c,v}(k)\frac{dk}{dE} = \frac{1}{2\pi^2}\left(\frac{2m^*_{c,v}}{\hbar^2}\right)^{3/2} E^{1/2} \tag{2.5}$$

The above expression gives the density of states for 3-dimensional (3-D) electrons and holes, *i.e.*, available k-states in the 3-D space are counted. In quantum well structures, where electrons and holes are confined to planes of motion, we instead count the 2-dimensional (2-D) availability of k-states and find that the 2-D density

of states (per unit energy and unit area) can be expressed as

$$\rho_{c,v}^{2D}(E) = \sum_{n=1}^{\infty} \frac{m_{c,v}^*}{\pi\hbar^2} H(E - E_{nc,v}) \tag{2.6}$$

where $H(x)$, the Heaviside function is equal to unity when $x > 0$ and is zero when $x < 0$, and where $E_{nc,v}$ is the eigen energy value for the n^{th} transverse quantum state in the conduction or valence band.

The density of states defines how many states exist for a given energy interval $E \rightarrow E + dE$. The probability that a given state is actually occupied by an electron is governed by the Fermi-Dirac law

$$f(E) = \frac{1}{1 + e^{(E-E_f)/k_B T}} \tag{2.7}$$

where E_f is the Fermi energy, k_B is the Boltzmann's constant and T is the temperature. In thermal equilibrium, a single Fermi energy applies to both conduction and valence bands. Under conditions in which the thermal equilibrium is disturbed, for example, by electrical pumping, two separate Fermi levels E_{fc} and E_{fv}, called quasi-Fermi levels, are used for each of the bands. In this case the electron density N and hole density P can be written as

$$N = \int_0^{\infty} f_c(E)\rho_c(E)dE \tag{2.8}$$

$$P = \int_0^{\infty} f_v(E)\rho_v(E)dE \tag{2.9}$$

To calculate the optical gain for a semiconductor system, we start from a two-level discrete atomic or electronic medium. Let us assume that the population densities of lower and upper levels are N_1 and N_2, respectively, and the energy difference between

the two levels is $\hbar\omega_0$. The complex susceptibility of such a system can be found using the density matrix formalism and it is given by [28]

$$\chi(\omega) = -\frac{\mu^2 T_2 (N_2 - N_1)[(\omega_0 - \omega)T_2 - i]}{\epsilon_0 \hbar [1 + (\omega - \omega_0)^2 T_2^2]} \tag{2.10}$$

where μ is the momentum matrix element and T_2 is a phenomenologically introduced dephasing time.

In a direct-gap semiconductor, the minimum in the conduction band and the maximum in the valence band occur at the same value of the wave vector $\mathbf{k}$. Since the photon carries negligible momentum compared with the carrier momentum $\hbar\mathbf{k}$, radiative transitions occur between electrons and holes of essentially same wave vectors. In the case of such a semiconductor system, modification to the density inversion $(N_2 - N_1)$ can be achieved by first considering the contribution from electrons with a value of the wave vector between k and $k + dk$. Their contribution to the density inversion is found to be

$$\begin{aligned} d(N_2 - N_1) &= \frac{1}{V}\rho(k)dk\{f_c(E_a)[1 - f_v(E_b)] - f_v(E_b)[1 - f_c(E_a)]\} \\ &= \frac{1}{V}\rho(k)dk[f_c(E_a) - f_v(E_b)] \end{aligned} \tag{2.11}$$

where $E_a = \hbar^2 k^2 / 2m_c^*$ and $E_b = \hbar^2 k^2 / 2m_v^*$ are the energy levels corresponding to the wave vector value k in the conduction and valence bands, respectively. Substituting Eq. (2.11) for $(N_2 - N_1)$ in Eq. (2.10) gives the total complex susceptibility in a semiconductor

$$\chi(\omega) = -\frac{1}{V}\int_0^\infty \frac{\mu^2 T_2[(\omega_0 - \omega)T_2 - i]}{\epsilon_0 \hbar [1 + (\omega - \omega_0)^2 T_2^2]}[f_c(E_a) - f_v(E_b)]\rho(k)dk \tag{2.12}$$

We note that there exists the following relation

$$\hbar\omega_0 = (E_c + E_a) - (E_v - E_b) = E_g + \hbar^2 k^2 / 2m_r^* \tag{2.13}$$

where E_c, E_v are energy levels of the conduction band minimum and the valence band maximum, respectively; $E_g = E_c - E_v$ is the band gap; and m_r^* is the reduced mass given by the relation $m_r^{*-1} = m_c^{*-1} + m_v^{*-1}$. Using Eqs. (2.3) and (2.13), we change the independent variable of Eq. (2.12) to ω_0 and obtain the following expression for the complex susceptibility

$$\chi(\omega) = -\frac{1}{\epsilon_0 \hbar} \int_{E_g/\hbar}^{\infty} \mu^2(\omega_0) T_2 \rho_j(\omega_0) \frac{(\omega_0 - \omega)T_2 - i}{1 + (\omega - \omega_0)^2 T_2^2} [f_c(\omega_0) - f_v(\omega_0)] d\omega_0 \tag{2.14}$$

where we have introduced the joint density of states $\rho_j(\omega_0)$, which is given by

$$\rho_j(\omega_0) = \frac{1}{2\pi^2} \left(\frac{2m_r^*}{\hbar} \right)^{3/2} (\omega_0 - E_g/\hbar)^{1/2} \tag{2.15}$$

In addition, the explicit expressions for the Fermi functions appearing in Eq. (2.14) are given by

$$f_c(\omega_0) = \frac{1}{1 + e^{[\frac{m_r^*}{m_c^*}(\hbar\omega_0 - E_g) + E_c - E_{fc}]/k_B T}} \tag{2.16}$$

$$f_v(\omega_0) = \frac{1}{1 + e^{[-\frac{m_r^*}{m_v^*}(\hbar\omega_0 - E_g) + E_v - E_{fv}]/k_B T}} \tag{2.17}$$

It follows that the gain constant can then be expressed as

$$\begin{aligned} \gamma(\omega) &= \frac{k}{n^2} \mathrm{Im}[\chi(\omega)] \\ &= \frac{k}{n^2 \epsilon_0 \hbar} \int_{E_g/\hbar}^{\infty} \mu^2(\omega_0) \rho_j(\omega_0) [f_c(\omega_0) - f_v(\omega_0)] \frac{T_2 d\omega_0}{1 + (\omega - \omega_0)^2 T_2^2} \end{aligned} \tag{2.18}$$

where n is refractive index of the semiconductor material and $k = \omega n/c$ is the wave number of the incident optical field at optical frequency $\omega/2\pi$. Since ω and $E_g/\hbar$ are

on the order of 10^{15} s^{-1}, and T_2^{-1} is typically on the order of 10^{13} s^{-1}, $\frac{T_2}{1+(\omega-\omega_0)^2T_2^2}$ can be approximated as $\pi\delta(\omega-\omega_0)$ when the integral in Eq. (2.18) is evaluated. This leads to

$$\gamma(\omega) = \frac{\mu^2}{\lambda\epsilon_0 n\hbar}\left(\frac{2m_r^*}{\hbar}\right)^{3/2}(\omega - E_g/\hbar)^{1/2}[f_c(\omega) - f_v(\omega)] \tag{2.19}$$

In a similar fashion, we can derive the gain constant for a pumped quantum well structure having a well thickness of L_z. It is given by

$$\gamma^{2D}(\omega) = \frac{2\pi\mu^2 m_r^*}{\lambda\epsilon_0 n\hbar^2 L_z}[f_c(\omega) - f_v(\omega)]\sum_{n=1}^{\infty} H[\hbar\omega - (E_g + E_{nc} + E_{nv})] \tag{2.20}$$

Eqs. (2.19) and (2.20) give a clear physical picture of optical gain in semiconductors. The necessary condition for net gain ($\gamma > 0$) in either case is that

$$f_c(\omega) - f_v(\omega) > 0 \tag{2.21}$$

If we use the Fermi functions given by Eqs. (2.16) and (2.17), the condition becomes

$$E_{fc} - E_{fv} > \hbar\omega \tag{2.22}$$

Eqs. (2.19) and (2.20) also indicate that the gain profile depends sensitively on many parameters. First, it depends on the carrier density N, which determines the quasi-Fermi energies for the carriers via Eqs. (2.8) and (2.9). These quasi-Fermi energy levels, in the context of the Fermi functions, determine the occupancy probability and is used in Eqs. (2.19) and (2.20) to calculate the gain. The carrier density can be varied by electrical injection or optical excitation. Under a given pumping condition, the carrier density can be calculated by solving a rate equation, as will be presented in the following section.

The gain profile also depends sensitively on the carrier temperature, which affects the Fermi distribution functions, as expressed in Eqs. (2.16) and (2.17). In the next section, saturation of semiconductor optical gain due to carrier temperature increase will be discussed.

2.3 Gain Saturation and Nonlinearities

Gain saturation, an important property of semiconductor lasers and amplifiers, can be understood using the rate equation analysis. The carrier density N at an injected current I and in the presence of optical power P can be obtained by solving the rate equation

$$\frac{dN}{dt} = \frac{I}{qV} - \frac{N}{\tau_s} - \frac{\gamma(N)}{A\hbar\omega}P + D\nabla^2 N \tag{2.23}$$

where q is the electron charge; V is the active layer volume, τ_s is the spontaneous carrier lifetime, $\gamma(N)$ is the gain constant per unit length as given by Eq. (2.19) or Eq. (2.20), A is the cross-section area of the optical guided mode and D is the carrier diffusion coefficient. This rate equation can be derived from the density matrix formalism combined with the rate equation approximation and can also be understood intuitively from the viewpoint of carrier number bookkeeping.

In the case of semiconductor optical amplifiers, the carrier density N is also a function of longitudinal location z. The solution of the above equation is complicated because of the presence of the diffusion term. The main effect of the carrier diffusion is to wash out the carrier gradient in the longitudinal direction. To a good degree of approximation, this term can be ignored in the case of traveling-wave amplifiers.

The carrier density N thus satisfies the simpler rate equation

$$\frac{dN}{dt} = \frac{I}{qV} - \frac{N}{\tau_s} - \frac{\gamma(N)}{A\hbar\omega}P \tag{2.24}$$

To simplify the solution of Eq. (2.24), the optical gain is assumed to vary linearly with the carrier density N, *i.e.*,

$$\gamma(N) = a(N - N_0) \tag{2.25}$$

where a is the differential gain and N_0 is the carrier density at which the active region becomes transparent. Under the condition of steady operation, *i.e.*, injection current I and optical power P are constant, the carrier density is found to be

$$N = \frac{I\tau_s/qV + N_0 P/P_s}{1 + P/P_s} \tag{2.26}$$

where P_s is the saturation power given by

$$P_s = \frac{A\hbar\omega}{a\tau_s} \tag{2.27}$$

Gain saturation behavior can thus be expressed

$$\gamma(N) = a(N - N_0) = \frac{a(I\tau_s/qV - N_0)}{1 + P/P_s} = \gamma_0 S \tag{2.28}$$

where $\gamma_0 = a(I\tau_s/qV - N_0)$ is the unsaturated optical gain in absence of input optical field, and where we have introduced a saturation factor S, which is a function of z and is given by

$$S(z) = \frac{1}{1 + P(z)/P_s} \tag{2.29}$$

Physically, the gain saturation is caused by stimulated emission through which carrier density is reduced by the input optical field. This saturation phenomenon,

usually referred to as interband gain saturation, has been extensively studied and well understood. There exists yet another type of gain saturation, resulting from various intraband processes. In this case, the occupation probability of the carriers in each energy band, rather than the actual carrier population, is altered by the input optical field. This leads to intraband gain saturation, also known as the nonlinear gain effect which is often phenomenologically represented by a nonlinear gain coefficient ϵ_p, as defined in the relation $\gamma(N,P) = \gamma(N,0)/(1+\epsilon_p P)$.

Intraband processes that cause gain nonlinearity typically include dynamic carrier heating and spectral hole burning. Dynamic carrier heating results from stimulated emission, which removes "cold" carriers close to the band edges, and free-carrier absorption, which transfers carriers to high energies within the bands. These nonthermal carriers thermalize among themselves via the intraband carrier-carrier scattering process on a time scale of < 100 fs. The hot carrier distributions relax to the lattice temperature by emission of optical phonons with a characteristic time constant of ~ 1 ps. For a fixed carrier density N, heating the carrier distribution will compress the optical gain, as can be understood by using Eq. (2.19) or Eq. (2.20), resulting in gain nonlinearity. The physical processes of dynamic carrier heating and gain profile change are illustrated in Figure 2.1.

Spectral hole burning, on the other hand, refers to a spectrally local gain reduction due to the input optical field. Stimulated emission removes carriers at states in the band corresponding to the photon energy. The carriers in neighboring states can not completely replenish the removed carriers due to finite intraband carrier-carrier

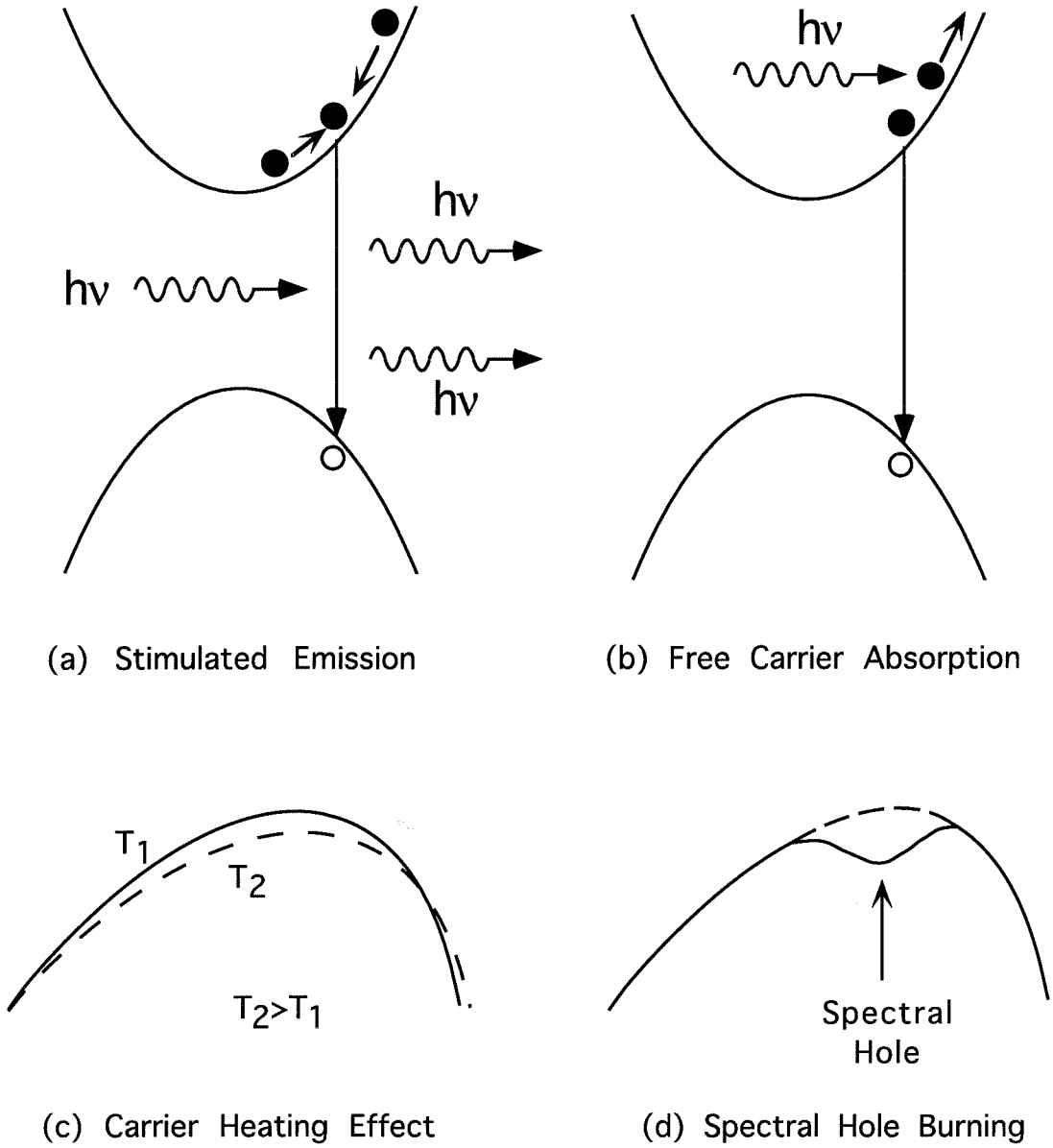

Figure 2.1: Illustration of physical processes involved in dynamic carrier heating and spectral hole burning.

scattering time ($<$ 100 fs), which sets the time scale on which non-Fermi carrier distributions are restored to equilibrium. This process creates a "hole" in the carrier distribution in the k-space and, consequently, a spectral hole in the gain profile. This is also illustrated in Figure 2.1.

Gain nonlinearities caused by intraband dynamics are intrinsically weak and gain reduction is usually much less than 1%. Such a small gain reduction barely affects the laser characteristics under continuous operation; however, owing to their ultrafast nature ($<$ 1 ps), intraband dynamics can greatly affect semiconductor laser dynamics, including noise properties and modulation dynamics [29]. For example, nonlinear gain introduces an additional damping to the relaxation oscillation in semiconductor laser modulation, severely limiting the maximum modulation bandwidth. In addition, these gain nonlinearities cause undesirable cross-talk for wavelength multiplexed signals in semiconductor optical amplifiers. On the other hand, however, they can be utilized to realize ultrafast switching, wavelength conversion and other useful nonlinear functionalities [23]–[26].

Bibliography

[1] R. N. Hall, G. E. Fenner, J. D. Kingley, T. J. Soltys, and R. O. Carlson, "Coherent light emission from GaAs junctions," *Phys. Rev. Lett.*, vol. 9, pp. 366-368, 1962.

[2] M. I. Nathan. W. P. Dumke, G. Burns, F. H. Dill, Jr., and G. Lasher, "Stimulated emission of radiation from GaAs p-n junctions," *Appl. Phys. Lett.*, vol. 1, pp. 62-64, 1962.

[3] N. Holonyak, Jr., and S. F. Bevacqua, "Coherent (visible) light emission from $Ga(As_{1-x}P_x)$ junctions," *Appl. Phys. Lett.*, vol. 1, pp. 82-83, 1962.

[4] T. M. Quist, R. H. Rediker, R. J. Keyes, W. E. Krag, B. Lax, A. L. McWhorter, and H. J. Zieger, "Semiconductor maser of GaAs," *Appl. Phys. Lett.*, vol. 1, pp. 91-92, 1962.

[5] H. Kressel and J. K. Butler, *Semiconductor Lasers and Heterojunction LED's*, Academic Press, 1977.

[6] H. C. Casey, Jr., and M. B. Panish, *Heterostructure Lasers: Part A*, Academic Press, 1978.

[7] G. P. Agrawal and N. K. Dutta, *Long-Wavelength Semiconductor Lasers*, van Nostrand Reinhold, 1986.

[8] P. S. Zory, Jr., Ed. *Quantum Well Lasers*, Academic Press, 1993.

[9] J. W. Crowe and R. M. Craig, Jr., "Small-signal amplification in GaAs lasers," *Appl. Phys. Lett.*, vol. 4, pp. 57, 1964.

[10] W. F. Kosonocky and R. H. Cornely, "GaAs laser amplifiers," *IEEE J. Quantum Electron.*, vol. 4, pp. 125, 1968.

[11] Y. Yamamoto, "Characteristics of AlGaAs Fabry-Perot cavity type laser amplifiers," *IEEE J. Quantum Electron.*, vol. 16, pp. 1047–1052, 1980.

[12] J. C. Simon, "Semiconductor laser amplifiers for single mode fiber communications," *J. Optical Commun.*, vol. 4, pp. 51–62, 1983.

[13] J. C. Simon, "GaInAsP semiconductor laser amplifiers for single mode fiber communications," *IEEE J. Lightwave Technol.*, vol. 5, pp. 1286–1295, 1987.

[14] M. J. O'Mahony, "Semiconductor-laser optical amplifiers for use in future fiber systems," *IEEE J. Lightwave Technol.*, vol. 6, pp. 531, 1988.

[15] N. A. Olsson, "Lightwave systems with optical amplifiers," *IEEE J. Lightwave Technol.*, vol. 7, pp. 1071–1082, 1989.

[16] T. Saitoh, T. Mukai, and O. Mikami, "Theoretical-analysis and fabrication of antireflection coatings on laser-diode facets," *IEEE J. Lightwave Technol.*, vol. 3, pp. 288–293, 1985.

[17] C. E. Zah, J. S. Osinski, C. Caneau, S. G. Menocal, L. A. Reith, J. Salzman, F. K. Shokoohi, and T. P. Lee, "Fabrication and performance of 1.5 μm GaInAsP traveling-wave laser-amplifiers with angled facets," *Electron. Lett.* vol. 23, pp. 990–992, 1987.

[18] N. A. Olsson, R. F. Kazarinov, W. A. Nordland, C. H. Henry, M. G. Oberg, H. G. White, P. A. Garbinski, and A. Savage, "Polarization-independent optical amplifier with buried facets," *Electron. Lett.*, vol. 25, pp. 1048–1049, 1989.

[19] N. A. Olsson and P. A. Garbinski, "High-sensitivity direct-detection receiver with a 1.5μm optical preamplifier," *Electron. Lett.*, vol. 22, pp. 1114–1116, 1986.

[20] M. G. Oberg, N. A. Olsson, L. A. Koszi, and G. J. Przybylek, "313-km transmission experiment at 1 Gbit/s using optical amplifiers and a low chirp laser," *Electron. Lett.*, vol. 24, pp. 38–39, 1988.

[21] W. I. Way, C. E. Zah and T. P. Lee, "Applications of traveling-wave laser-amplifiers in subcarrier multiplexed lightwave systems," *IEEE Trans. Microwave Theory Tech.*, vol. 38, pp. 534–545, 1990.

[22] T. Li, "The impact of optical amplifiers on long-distance lightwave telecommunications," *Proc. IEEE*, vol. 81, pp. 1633–1646, 1993.

[23] M. C. Tatham, G. Sherlock, and L. D. Westbrook, "20 nm wavelength conversion using nondegenerate four-wave mixing," *IEEE Photon. Tech. Lett.*, vol. 5, pp. 1303–1306, 1993.

[24] J. Zhou, N. Park, K. J. Vahala, M. A. Newkirk, and B. I. Miller, "Four-wave mixing wavelength conversion efficiency in semiconductor traveling-wave amplifiers measured to 65 nm of wavelength shift," *IEEE Photon. Technol. Lett.*, vol. 6, pp. 984–987, 1994.

[25] L. E. Adams, E. S. Kintzer, and J. G. Fujimoto, "All-optical clock recovery using a modelocked figure eight laser with a semiconductor nonlinearity," *Electron. Lett.*, vol. 30, pp. 1696–1697, 1994.

[26] S. Shimada, K. Nakagawa, M. Saruwatari, and T. Matsumoto, "Very-high-speed optical signal processing," *Proc. IEEE*, vol. 81, pp. 1633–1646, 1993.

[27] T. L. Koch and U. Koren, "Semiconductor photonic integrated-circuits," *IEEE J. Quantum Electron.*, vol. 27, pp. 641–653, 1991.

[28] A. Yariv, *Quantum Electronics*, 3rd Ed., chapter 8, John Wiley & Sons, 1989.

[29] G. P. Agrawal and G. R. Gray, "Importance of nonlinear gain in semiconductor lasers," *SPIE Proc.*, vol. 1497, pp. 444–455, 1991.

Chapter 3

Four-Wave Mixing in Semiconductor Optical Amplifiers

3.1 Introduction

Nondegenerate four-wave mixing in semiconductor optical amplifiers (SOA's) has been a topic of increasing interest over the past few years. Four-wave mixing has been demonstrated as an effective frequency-domain tool to probe ultrafast semiconductor dynamics [1]–[5]. It has also be studied for applications in lightwave systems, including wavelength conversion [6]–[8], all-optical demultiplexing of high bit-rate time-division-multiplexed signals [9] and all-optical conversion from time-division-multiplexing to wavelength-division-multiplexing [10].

Physical mechanisms responsible for four-wave mixing are interband gain saturation, arising from stimulated emission, and intraband gain nonlinearities, resulting from intraband dynamics. In the former case, carrier density is modulated by the op-

tical beating of pump and probe, while in the latter case, the carrier density remains unchanged but intraband occupancy probability is modulated. Both mechanisms can create dynamic gain and index gratings along the amplifier length. The subsequent scattering of pump and probe fields from these gratings results in the generation of two new side bands. This is the basic process of four-wave mixing in SOA's.

In the next section, the theory concerning four-wave mixing in SOA's is presented which includes contributions to four-wave mixing from both interband and intraband dynamics. Experimental investigation of using four-wave mixing to probe ultrafast intraband dynamics will be presented in the next chapter.

3.2 Theoretical Analysis

Four-wave mixing in a semiconductor medium generated by intraband occupancy modulation was first analyzed by Agrawal [11]. His theory, based on the density-matrix equations, included contributions from interband carrier density modulation and spectral hole burning. A recently published paper by Uskov *et al.* [12], also based on density-matrix approach, included both carrier heating and spectral hole burning. In this chapter, we use some results from the above referenced work and put our emphasis on an analytical solution to the coupled equations. We also address some practical issues such as the phase matching condition.

Let us assume that the pump, probe and the four-wave mixing signal all have the same polarization, and that these guided waves are given by

$$\mathcal{E}_j(z,t) = E_j(z) \exp\left[i(k_j z - \omega_j t)\right] \tag{3.1}$$

where $j = p, q, s$ denote pump, probe and four-wave mixing signals, respectively; and $\{E_j(z)\}$ are the slowly-varying amplitudes of the three waves.

The interband and intraband photomixing of pump and probe waves in the active layer will of course influence the propagation of the four-wave mixing signal wave, as well as the pump and probe waves themselves. We can describe the propagation of these waves by means of coupled-amplitude equations. Assuming the validility of the slowly-varying-amplitude approach, and following procedures similar to those used in Agrawal's treatment [11], we find that the slowly varying amplitudes must obey the following set of coupled equations

$$\frac{dE_{p,q}(z)}{dz} = \frac{1}{2}\left[g_0\, S(z)\,(1-i\alpha) - \alpha_l\right] E_{p,q}(z) \tag{3.2}$$

$$\frac{dE_s(z)}{dz} = \frac{1}{2}\left[g_0\, S(z)\,(1-i\alpha) - \alpha_l\right] E_s(z) - \kappa(z)\, E_p^2(z)\, E_q^*(z)\, \exp(i\Delta k z) \tag{3.3}$$

where we have introduced a wave-number mismatch $\Delta k = 2k_p - k_q - k_s$ and a four-wave mixing coupling coefficient $\kappa(z)$. In addition, g_0 is the unsaturated optical gain per unit length, with its wavelength dependence neglected. g_0 is related to the gain constant γ_0 by $g_0 = \Gamma\gamma_0$, with Γ being the optical confinement factor. α is the linewidth enhancement factor; α_l is the SOA's nonsaturable internal loss per unit length; and $P(z)$ is the total optical power at position z in the waveguide.

Eq. (3.2) is a simple amplification rate equation where we have neglected the power depletion of pump and probe waves, since, for detuning frequencies larger than a few tens of GHz, the power transfer is negligible in comparison to the power in the pump and probe themselves. In Eq. (3.3), while the first term is the normal amplifi-

cation term, the second term is a nonlinear mixing term giving energy coupling from pump and probe to the four-wave mixing signal frequency. The coupling coefficient $\kappa(z)$ measures the strength of this nonlinear mixing precess, and it is related to the conventional third-order nonlinear coefficient $\chi^{(3)}$ by $\kappa = -i\frac{\omega}{2}\sqrt{\frac{\mu_0}{\epsilon}}\chi^{(3)}$.

The coupling coefficient $\kappa(z)$ is of central importance to this theoretical analysis. To simplify the analysis, we treat the three contributing mechanisms – carrier density modulation, dynamic carrier heating and spectral hole burning – as three independent processes. $\kappa(z)$ can then be decomposed as

$$\kappa(z) = \sum_{j=1}^{3} \kappa_j(z) \tag{3.4}$$

with $j = 1, 2, 3$ denoting carrier density modulation, dynamic carrier heating and spectral hole burning, respectively.

Although a formal justification of this assumption is possible based on the density matrix formalism [12], the separation of the three mechanisms can be justified intuitively by noting that, first, all interactions measured are in the small-signal regime in our four-wave mixing studies and, secondly, each relaxation mechanism results from bath damping from distinct, independent baths (κ_1 – photon continuum, κ_2 – phonon continuum, and κ_3 – carrier eigenstate continuum).

The first and third terms in Eq. (3.4) are due to carrier density modulation and spectral hole burning, respectively. They can be found by solving the density matrix equations and evaluating the induced polarization at the four-wave mixing signal frequency [11]. Their expressions are given by

$$\kappa_j(z) = \frac{1}{2} \cdot g_0 S(z) \cdot \frac{1 - i\alpha_j}{P_j} \cdot \frac{1}{1 - i2\pi f \tau_j} \qquad \text{j} = 1 \text{ or } 3 \tag{3.5}$$

where $\tau_1 = \tau_s S$ is the effective carrier lifetime; α_1 is the linewidth enhancement fact α; P_1 is the interband saturation power P_s; and τ_3 and P_3 are the intraband population relaxation lifetime and saturation power associated with spectral hole burning.

The spectral hole burning saturation power P_3 is related to the dipole matrix element, the dipole dephasing relaxation time and intraband population relaxation lifetime through the expression $\hbar^2/\mu^2 T_2 \tau_3$ [11]. It is important to note that P_3 is much greater than the ordinary saturation power P_1, since, physically, the gain saturation due to intraband processes is much weaker than the saturation induced in the carrier density. The parameter α_3 is the ratio of real and imaginary parts of the refractive index change caused by spectral hole burning, and it should usually have a value much smaller than unity [11]. Additionally, in Eq. (3.5) for j=3, we have made use of the fact that the dipole dephasing relaxation time T_2 is much shorter than the intraband population relaxation time τ_3.

The second term in Eq. (3.4) represents the contribution from dynamic carrier heating. Dynamic carrier heating includes at least two processes. The carriers are heated through a combination of free-carrier absorption and stimulated emission, as discussed in the previous chapter. These nonequilibrium carriers then thermalize on a time scale of $\tau_3 < 100$ fs, and in the meanwhile, the hot carriers relax to the lattice temperature by emission of optical phonons. Because the heating and cooling processes occur on very different time scales ($\sim$ 1 ps versus $<$ 100 fs), we can treat them as two distinctive processes: initial heating and subsequent cooling.

The cooling process, which can be regarded as a thermal process, can be char-

acterized with a relaxation (cooling) time constant τ_2. However, it is intrinsically more complicated to model the nonthermal heating process. Because our four-wave mixing studies are in the small-signal regime, we can assign a "virtual" temperature to the nonthermal carrier distribution and assume that the δ function response of the initialization process follows $(1 - e^{-t/\tau_3})$, where τ_3 is the intraband carrier-carrier scattering time constant.

The initial carrier heating process can then be described by the following equation

$$T(t) - T(-\infty) = -\int_{-\infty}^{t} \frac{T(t_1) - T_l}{\tau_2}\, dt_1 + H\int_{-\infty}^{t} \left(1 - e^{-\frac{t-t_1}{\tau_3}}\right) P(t_1)\, dt_1 \qquad (3.6)$$

where $T(t)$ is carrier temperature (electrons and holes are assumed to have same temperature) and T_l is the lattice temperature. H is the heating coefficient, defined as carrier temperature increase caused by unit optical power in unit time interval, and it is determined by the contributing heating mechanisms. Eq. (3.6) can be reduced to

$$\frac{d^2T(t)}{dt^2} + (\frac{1}{\tau_2} + \frac{1}{\tau_3})\frac{dT(t)}{dt} + \frac{T(t) - T_l}{\tau_2\tau_3} = H\frac{P(t)}{\tau_3} \qquad (3.7)$$

Solving the above equation and following similar procedures as in the derivation of $\kappa_1(z)$, we obtain the expression for $\kappa_2(z)$

$$\kappa_2(z) = \frac{1}{2} \cdot g_0 S(z) \cdot \frac{1 - i\alpha_2}{P_2} \cdot \left(\frac{1}{1 - i2\pi f\tau_2} - \frac{\tau_3}{\tau_2} \cdot \frac{1}{1 - i2\pi f\tau_3}\right) \qquad (3.8)$$

where P_2 is the saturation power for the carrier heating effect and is related to the carrier relaxation (cooling) time τ_2 and the differential gain with respect to the carrier temperature. Like the saturation power associated with spectral hole burning P_3, the saturation power P_2 is much larger than the ordinary saturation power P_1. In

addition, α_2 is the ratio of the real and the imaginary parts of the refractive index change induced by dynamic carrier heating. Both interband transitions and electron-hole plasma absorption may contribute to this parameter.

We can now write an expression for $\kappa(z)$

$$\begin{aligned}\kappa(z) &= \frac{1}{2}\cdot g_0 S(z)\cdot\left[\frac{1-i\alpha_1}{P_1}\cdot\frac{1}{1-i2\pi f\tau_1}+\frac{1-i\alpha_2}{P_2}\cdot\frac{1}{1-i2\pi f\tau_2}\right.\\ &\left.+\left(\frac{1-i\alpha_3}{P_3}-\frac{\tau_3}{\tau_2}\cdot\frac{1-i\alpha_2}{P_2}\right)\cdot\frac{1}{1-i2\pi f\tau_3}\right] \qquad (3.9)\end{aligned}$$

Physically, the first term represents carrier density modulation; the second term represents the relaxation (cooling) process of the dynamic carrier heating effect; the third term represents the intraband carrier-carrier scattering process, with first part for spectral hole burning and second part for the initial heating process associated with the dynamic carrier heating.

To solve the differential equations, we first rewrite Eq. (3.2) as:

$$E_{p,q}(z) = E_{p,q}(0)\exp\left\{\int_0^z \frac{1}{2}\left[g_0 S(z_1)\cdot(1-i\alpha_1)-\alpha_l\right]dz_1\right\} \qquad (3.10)$$

Substituting Eq. (3.10) into Eq. (3.3) gives

$$\begin{aligned}\frac{dE_s(z)}{dz} &= \frac{1}{2}\left[g_0 S(z)\cdot(1-i\alpha_1)-\alpha_l\right]E_s(z)-\kappa(z)E_p^2(0)E_q^*(0)\\ &\cdot\exp\left\{\int_0^z\left[\left(\frac{3}{2}g_0-i\frac{1}{2}g_0\alpha_1\right)S(z)-\frac{3}{2}\alpha_l+i\triangle k\right]dz_1\right\} \qquad (3.11)\end{aligned}$$

Using the boundary condition $E_s(0)=0$, the solution to Eq. (3.11) is found to be

$$\begin{aligned}E_s(z) &= -E_p^2(0)E_q^*(0)\int_0^z \kappa(z_1)\exp\left[R(z_1)z_1\right]dz_1\\ &\cdot\exp\left\{\int_0^z\frac{1}{2}\left[g_0 S(z)\cdot(1-i\alpha_1)-\alpha_l\right]dz_1\right\} \qquad (3.12)\end{aligned}$$

where $R(z_1)$ is given by

$$R(z_1) = i\triangle k - \alpha_l + \frac{1}{z_1}\int_0^{z_1} g_0 S(z_2) dz_2 \tag{3.13}$$

Let us examine the integral $\int_0^z \kappa(z_1) e^{R(z_1)z_1} dz_1$ which appears in Eq. (3.12). The first part of the integrand $\kappa(z_1)$ is proportional to $S(z_1)$ as indicated in Eq. (3.9), and is therefore a slowly-decreasing function of z_1. The second part is an exponentially growing function with a complex growth rate of $R(z_1)$, which, as indicated in Eq. (3.13), is also a slowly varying function of z_1. Therefore, the dominant contribution to the integral comes from the interval near $z_1 = z$, and, when $E_s(l)$ is evaluated, the integrand can be approximated by $\kappa(l)\exp[R(l)z_1]$

Following the above approximations, $E_s(l)$ is found to be

$$E_s(l) = -\frac{E_p^2(l)E_q^*(l)\kappa(l)le^{i\triangle kl}}{0.23G + i\triangle kl} \tag{3.14}$$

where $G = 10(\log e)\int_0^l [g_0 S(z) - \alpha_l]dz$ is the SOA's saturated optical gain in dB. The underestimation of the four-wave mixing signal $E_s(l)$ introduced by the approximations depends on the SOA saturation level, and it is usually negligible for moderately saturated SOA's.

The second term accounts for the phase mismatch caused by material dispersion and waveguide dispersion. The phase mismatch can be expressed as

$$\triangle kl = \frac{2\pi\lambda^2 f^2}{c^2} \cdot \frac{dn_g}{d\lambda} \cdot l \tag{3.15}$$

where $\frac{dn_g}{d\lambda}$ is the group index dispersion. Using $\frac{dn_g}{d\lambda} \approx -0.7\ \mu\text{m}^{-1}$, measured by Hall *et al.* [13], and $l = 650\ \mu$m, the phase mismatch at $f = 1.7$ THz is estimated to be -0.22, which can be ignored in comparison with the first term for a typical SOA gain

of about 15 dB. Even for a detuning frequency up to 4 THz, the phase mismatch, -1.21, can be ignored, since, as shown in Eq. (3.14), the four-wave mixing signal power is proportional to $[(\text{first term})^2 + (\triangle kl)^2]^{-1}$.

3.3 Discussion

As indicated in Eqs. (3.9) and (3.14), the four-wave mixing signal power as a function of detuning frequency gives essentially the frequency-domain response function of the contributing semiconductor dynamics. Quantitative characterization of the four-wave mixing spectra can therefore provide important information concerning these dynamics. Previously, its time-domain counterpart, pump-probe measurement using ultra-short optical pulses [14]–[16] has been the only direct technique to probe ultrafast dynamics in semiconductor active layers. Four-wave mixing spectroscopy of semiconductor dynamics presents data in a form that is complementary to these femtosecond studies, *i.e.* frequency-domain versus time-domain. Experimental implementation of this frequency-domain technique to probe semiconductor dynamics will be detailed in the next chapter.

Physically, the term $\kappa(l)E_p(l)E_q^*(l)$ in Eq. (3.14) represents the strength of the dynamic gratings induced by optical beating of pump and probe fields. An additional factor of $E_p(l)$ arises from the fact that the four-wave mixing signal is generated through the scattering of the pump wave from these dynamic gratings. Since both pump and probe experience an optical gain of G, the SOA's single-pass gain acts three times in the expression for the four-wave mixing signal $E_s(l)$. This point is

critical to implementation of efficient broadband wavelength conversion in SOA's. We will experimentally illustrate this point in our experimental study of broadband wavelength conversion described in Chapter 6.

Bibliography

[1] L. F. Tiemeijer, "Effects of nonlinear gain on four-wave mixing and asymmetric gain saturation in a semiconductor laser amplifier," *Appl. Phys. Lett.*, vol. 59, pp. 499–501, 1991.

[2] K. Kikuchi, M. Kakui, C. E. Zah, and T. P. Lee, "Observation of highly nondegenerate four-wave mixing in a 1.5 μm traveling-wave semiconductor optical amplifier and estimation of nonlinear gain coefficient," *IEEE J. Quantum Electron.*, vol. 28, pp. 151–156, 1992.

[3] J. Zhou, N. Park, J. W. Dawson, K. J. Vahala, M. A. Newkirk, U. Koren, and B. I. Miller, "Highly nondegenerate four-wave mixing and gain nonlinearity in a strained multiple-quantum-well optical amplifier," *Appl. Phys. Lett.*, vol. 62, pp. 2301–2303, 1993.

[4] J. Zhou, N. Park, J. W. Dawson, K. J. Vahala, M. A. Newkirk, and B. I. Miller, "Terahertz four-wave mixing spectroscopy for study of ultrafast dynamics in a semiconductor optical amplifier," *Appl. Phys. Lett.*, vol. 63, pp. 1179–1181, 1993.

[5] J. Zhou, N. Park, K. J. Vahala, M. A. Newkirk, and B. I. Miller, "Study of inter-well carrier transport by terahertz four-wave mixing in an optical amplifier with tensile and compressively strained quantum wells," *Appl. Phys. Lett.*, vol. 65, pp. 1897–1899, 1994.

[6] M. C. Tatham, G. Sherlock, and L. D. Westbrook, "20 nm wavelength conversion using nondegenerate four-wave mixing," *IEEE Photon. Technol. Lett.*, vol. 5, pp. 1303–1306, 1993.

[7] J. Zhou, N. Park, K. J. Vahala, M. A. Newkirk, and B. I. Miller, "Broadband wavelength conversion with amplification by four-wave mixing in semiconductor traveling-wave amplifiers," *Electron. Lett.*, vol. 30, pp. 859-860, 1994.

[8] J. Zhou, N. Park, K. J. Vahala, M. A. Newkirk, and B. I. Miller, "Four-wave mixing wavelength conversion efficiency in semiconductor traveling-wave amplifiers measured to 65 nm of wavelength shift," *IEEE Photon. Technol. Lett.*, vol. 6, pp. 984–987, 1994.

[9] S. Kawanishi, T. Morioka, O. Kamatani, H. Takara, J. M. Jacob, and M. Saruwatari, "100 Gbit/s all-optical demultiplexing using four-wave mixing in a traveling-wave laser-diode amplifier," *Electron. Lett.*, vol. 30, pp. 981–982, 1994.

[10] M. A. Summerfield, J. P. R. Lacey, A. J. Lowery, and R. S. Tucker, "All-optical TDM to WDM conversion in a semiconductor optical amplifier," *Electron. Lett.*, vol. 30, pp. 255–256, 1994.

[11] G. P. Agrawal, "Population pulsations and nondegenerate four-wave mixing in semiconductor lasers and amplifiers," *J. Opt. Soc. Am. B*, vol. 5, pp. 147–158, 1988.

[12] A. Uskov, J. Mϕrk, and J. Mark, "Wave mixing in semiconductor laser amplifiers due to carrier heating and spectral hole burning," *IEEE J. Quantum Electron.*, vol. 30, pp. 1769–1781, 1994.

[13] K. L. Hall, G. Lenz, and E. P. Ippen, "Femtosecond time domain measurements of group velocity dispersion in diode lasers at 1.5 μm," *IEEE J. Lightwave Technol.*, vol. 10, pp. 616–619, 1992.

[14] K. L. Hall, J. Mark, E. P. Ippen, and G. Eisenstein, "Femtosecond gain dynamics in InGaAsP optical amplifiers," *Appl. Phys. Lett.*, vol. 56, pp. 1740–1742, 1990.

[15] J. Mark and J. Mϕrk, "Subpicosecond gain dynamics in InGaAsP optical amplifiers: experiment and theory," *Appl. Phys. Lett.*, vol. 61, pp. 9–11, 1992.

[16] K. L. Hall, G. Lenz, E. P. Ippen, U. Koren, and G. Raybon, "Carrier heating and spectral hole burning in strained-layer quantum-well laser amplifiers at 1.5 μm," *Appl. Phys. Lett.*, vol. 61, pp. 2512–2514, 1992.

Chapter 4

Terahertz Four-Wave Mixing Spectroscopy of Intraband Dynamics

4.1 Introduction

As discussed in the previous chapter, four-wave mixing in semiconductor optical amplifiers (SOA's) can be used as a spectroscopic tool for analysis of intraband dynamics in semiconductor active layers. Important information regarding these dynamics such as relaxation time constants can be extracted from analysis of measured four-wave mixing signal spectra, *i.e.*, four-wave mixing signal power versus detuning frequency.

Early four-wave mixing experiments were limited to detuning frequencies of a few hundred GHz [1]–[3]. For example, in an experiment reported by Tiemeijer [1], the four-wave mixing response was found to be consistent with carrier heating, but the

equivalent temporal resolution of the experiment, related to the maximum detuning frequency f_{max} by $1/2\pi f_{max}$, was not sufficient to resolve spectral hole burning. In another study [2], only spectral hole burning was inferred from the data, but no time constant was determined, also owing to the limited detuning frequency in the experiment.

The first four-wave mixing experiment that extended detuning frequencies into THz regime was performed in our group [4]. The maximum detuning in this study was as large as 1.7 THz, which corresponds to a sub-100 fs equivalent temporal resolution (94 fs). Contributions to four-wave mixing from both carrier heating and intraband carrier-carrier scattering were observed for the first time. This chapter presents the details of this experiment and a discussion of the experimental results. Since then, a number of similar experiments with THz detuning frequencies have been reported by other research groups and these studies also confirmed the simultaneous presence of carrier heating and spectral hole burning [5],[6]. In addition, we have recently developed a novel four-wave mixing configuration [7] to study inter-well carrier transport in semiconductor quantum well amplifiers. This work will be detailed in the next chapter.

4.2 Four-Wave Mixing Measurements

In order to perform four-wave mixing spectroscopic measurements in an SOA, there are some basic experimental requirements that must be met. First of all, two single-frequency lasers are needed for the pump and probe sources, and at least one of them

must be tunable. In our four-wave mixing studies, we used 1.5 μm, single frequency, widely tunable Erbium-doped fiber ring lasers [8]. These ring lasers are unidirectional laser oscillators in which fiber optical isolators are used to make the laser to operate in one direction and two tunable fiber Fabry-Perot (FFP) filters are employed as both wavelength selecting and tuning components.

Figure 4.1 illustrates the schematic diagram of the fiber laser structure and the concept of cascaded narrowband (free spectral range 6 GHz, finesse 100) and broadband (free spectral range 4 THz, finesse 100) FFP filters. These two cascaded FFP filters forced the laser to lase in a single longitudinal mode. Polarization controllers and a pigtailed polarizer were used to control the polarization state of the laser, as well as to eliminate the competition between different polarization modes. The laser output was coupled out of the resonator through a fiber optic bidirectional coupler. Typical output power was in the range of 1 $\sim$ 2 mW, depending on the lasing wavelength and pump power. The side-mode suppression and laser linewidth were measured to be about 70 dB and 4 kHz, respectively [9]. By electrically tuning the broadband FFP filter, the laser wavelength can be tuned over $\sim$ 30 nm, corresponding to the free spectral range of the broadband FFP filter. These characteristics make these fiber lasers ideal sources for the four-wave mixing studies.

The SOA's used in this four-wave mixing study were tensile strained or compressively strained InGaAs/InGaAsP multiple quantum well traveling amplifiers operating in the spectrum of 1.5 μm. They were designed and fabricated by M. A. Newkirk and B. I. Miller at AT&T Bell Laboratories [10],[11].

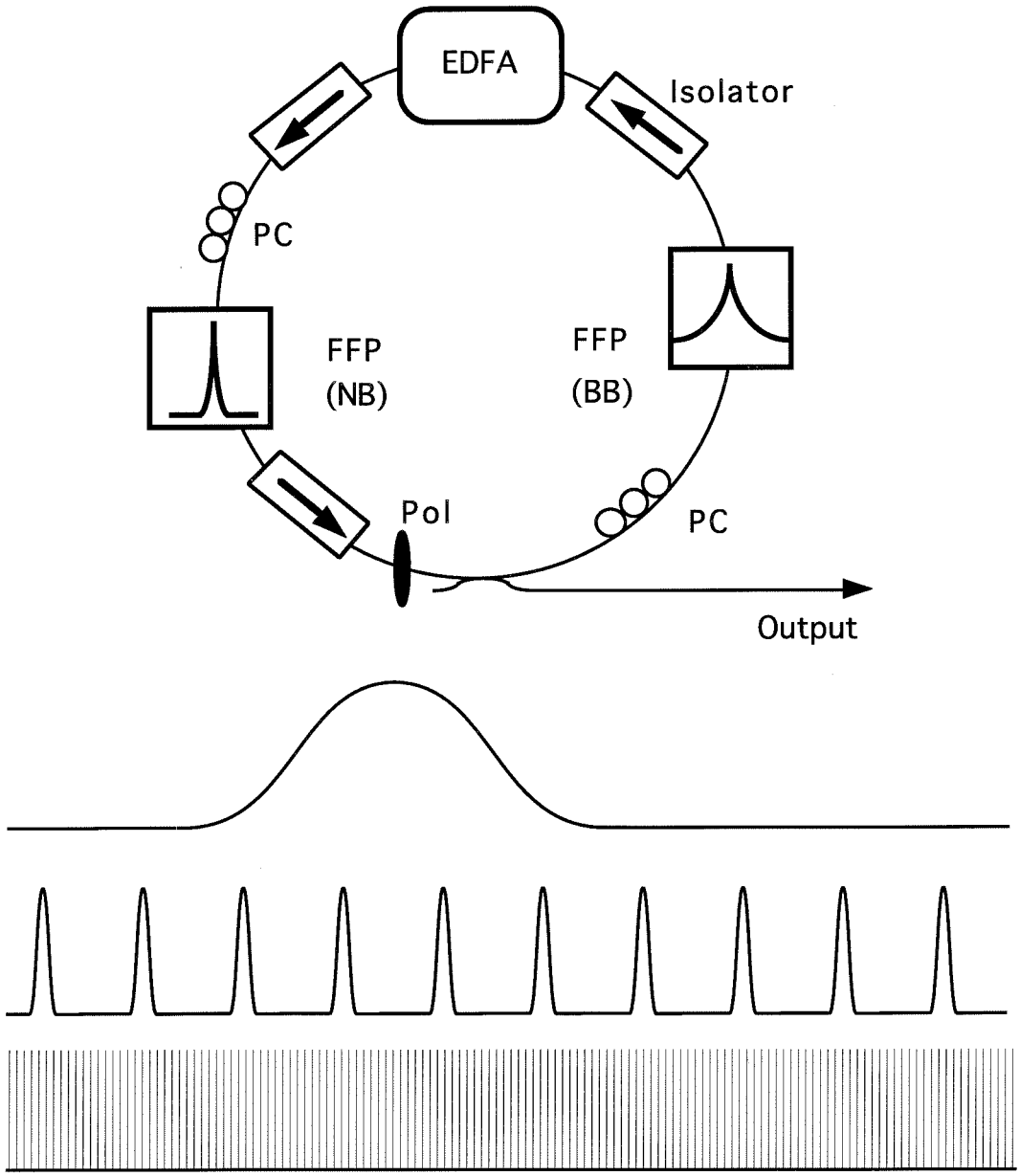

Figure 4.1: Schematic structure of the Erbium-doped fiber ring lasers used in the experiment and mechanism of mode selection (upper: broadband FFP mode; middle: narrowband FFP modes; lower: cavity modes).

The band diagram of the tensile strained amplifier [10] is shown in Figure 4.2. The structure was grown by atmospheric pressure metalorganic vapor phase epitaxy (MOVPE). The wells and barriers were approximately 160 and 270 Å thick, respectively. The wells were $In_{0.39}Ga_{0.61}As$ and were under tensile strain of 1%. The barriers were compressively strained InGaAsP ($E_g = 0.95$ eV) with about 0.15% of strain to partially compensate the tension in the wells. After the growth of the wafers, optical amplifiers were made using two additional MOVPE regrowths for blocking layers and p-type cladding layers. The amplifiers had 650 μm long gain sections and $20 - 40$ μm long window sections at both ends adjacent to the facets. Single SiO layers were used for anti-reflection coatings on the facets. The residual reflectivities of these amplifiers were estimated to be about 8×10^{-5}. The small signal gain of this tensile strained amplifier measured at several bias currents is also shown in Figure 4.2. High optical gain (> 20 dB) for TM-polarized input was obtained and gain ripple was negligible (< 0.2 dB). We also found in the measurements that the TE gain was very low, about 15 dB below the TM gain at 150 mA.

The compressively strained amplifier [11] was also grown using MOVPE. The base wafer comprises a strain-compensated 1.5 μm wavelength multiple quantum well gain layer on top of a 2800 Å thick InGaAsP passive waveguide. A three quantum well stack is composed of six 30 Å thick InGaAs wells with 1.3% compressive strain separated by 125 Å thick InGaAsP barriers ($E_g = 1.0$ eV) having 0.2% tensile strain. The device used the semi-insulating planar buried-heterostructure configuration. 3 μm wide mesas were created by standard photolithography and wet chemical etching,

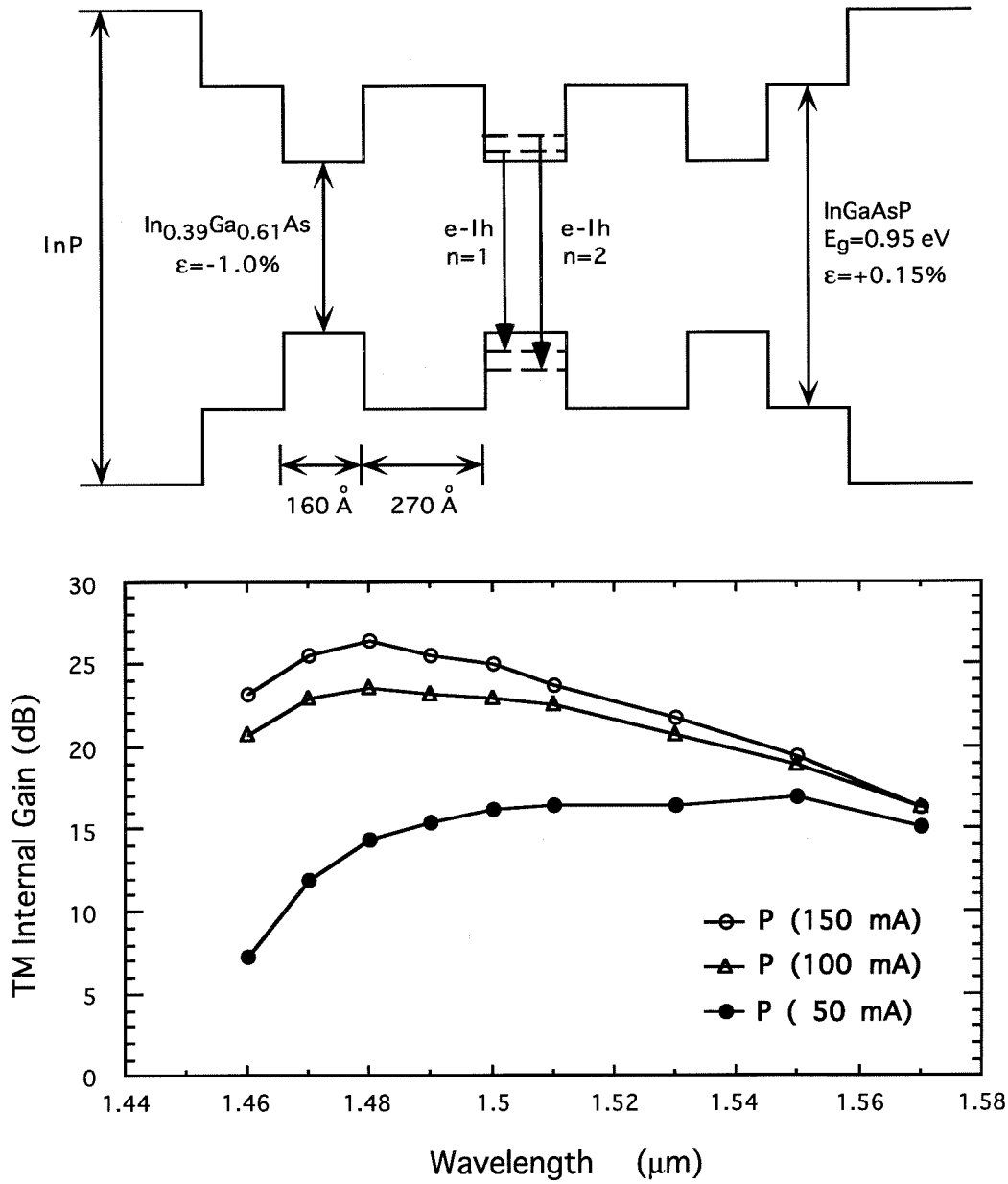

Figure 4.2: Upper figure illustrates the band diagram of the tensile strained amplifiers used in the experiment. Lower figure shows the small signal gain of the amplifiers at several pump currents.

followed by two MOVPE regrowths for current blocking, cladding and p-type contacting layers. The compressively strained amplifiers had a similar window structure for suppressing the facet reflectivity. The small signal gain at 1.55 μm for 150 mA bias current was measured to be about 16.3 dB with negligible gain ripple.

A typical experimental setup for THz four-wave mixing spectroscopy is shown in Figure 4.3. The optical outputs from the pump and probe fiber lasers were combined using a 3 dB fiber coupler, and then coupled into the SOA using microscope objectives. The optical power coupled into the SOA was about 250 μW. Two fiber polarization controllers were employed to match the polarization state of input pump and probe to a specific SOA polarization mode, *i.e.*, TM polarization for the tensile SOA, TE polarization for the compressive SOA. Two optical isolators were placed before and after the SOA to eliminate feedback caused by the facets of the input and output fibers, and also to serve as polarization selectors.

During the measurements, the pump laser wavelength was fixed at 1534 nm, while the probe was tuned to vary the detuning frequency f. The four-wave mixing signal was measured by a high-sensitivity heterodyne detection system, as illustrated in Figure 4.3, in which the four-wave mixing signal was mixed with a tunable fiber laser local oscillator using a beam splitter/combiner. This local oscillator was tuned relative to the signal frequency to generate an IF beating note at the *pin* detector, and the IF mixing frequency was maintained at a constant value of 4.00 GHz throughout the measurements. This ensured that the frequency response of detection electronics would not affect the measured results. The detected photocurrent was amplified

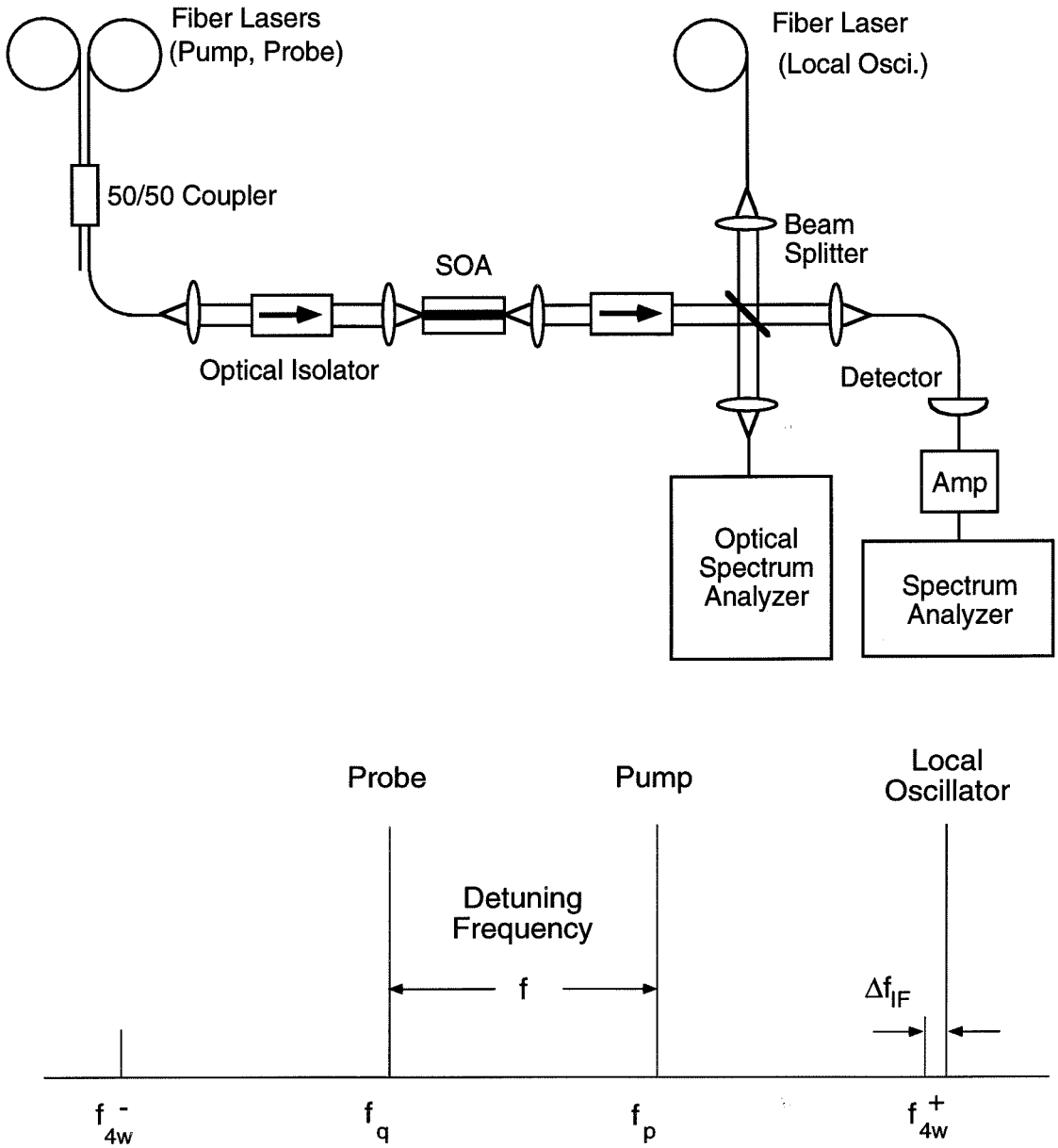

Figure 4.3: Schematic diagram of the experimental arrangement for four-wave mixing spectroscopy of intraband dynamics. The lower figure shows the concept of a high-sensitivity heterodyne detection system.

by a microwave amplifier with 40 dB gain and then measured using a spectrum analyzer (Tektronix 2782). The detuning frequencies were determined using an optical spectrum analyzer (Hewlett-Packard 70950A). Optical powers of the pump, probe and local oscillator were also measured, so that the measured four-wave mixing signal could be normalized.

4.3 Analysis of Experimental Results

Using the experimental configuration as shown in Figure 4.3, the four-wave mixing signal was measured for both the tensile and compressively strained SOA's. The largest detuning frequency in the measurements was 1.7 THz, limited only by the tunability of one of the fiber lasers used in the experiment. The signal level at the maximum detuning frequency was still $10 \sim 20$ dB above the noise floor, owing to the narrow linewidth and low intensity noise of the fiber lasers. The normalized signal power as a function of detuning frequency is illustrated in Figure 4.4 where a tensile strained SOA was measured, and in Figure 4.5 where a compressively strained SOA was measured.

To understand the experimental data, we first need an explicit expression for the four-wave mixing signal power as a function of the detuning frequency. Using Eqs. (3.9) and (3.14), the expression for the four-wave mixing signal power can be written as

$$P_{FWM} = P_p^2 P_q \mid \sum_{j=1}^{3} C_j \cdot \frac{1}{1 - i2\pi f \tau_j} \mid^2 \tag{4.1}$$

where P_p and P_q are powers of pump and probe at the SOA output; $\{C_j\}$ are complex

coupling coefficients representing contribution to four-wave mixing from carrier density modulation, carrier heating and intraband carrier-carrier scattering, respectively. They are given by

$$\begin{aligned} C_j &= -\frac{g_0 S(l) l}{0.46G} \cdot \frac{1 - i\alpha_j}{P_j} \qquad \text{for j = 1, 2} \\ C_3 &= -\frac{g_0 S(l) l}{0.46G} \cdot \left(\frac{1 - i\alpha_3}{P_3} - \frac{\tau_3}{\tau_2} \cdot \frac{1 - i\alpha_2}{P_2} \right) \end{aligned} \tag{4.2}$$

We then use Eq. (4.1) to fit the experimental data. The dashed line in Figure 4.4 represents the four-wave mixing response accounting only for carrier density modulation, *i.e.*, only the first term in Eq. (4.1) is used. As shown in Figure 4.4, this one term fit apparently can not explain the measured data. The deviation of the measured response from this one term fit indicates the presence of contributions from the intraband relaxation mechanisms. In addition, the asymmetric nature of the four-wave mixing signal spectrum with respect to positive and negative detuning is believed to result from phase interferences which occur between the various contributing mechanisms. Since the positive detuning data show constructive interferences, we estimated a relaxation time constant of about 650 fs for an ultrafast intraband mechanism using the positive signal spectrum. We then fit the measured data with these two terms. However, as shown in Figure 4.4, the two term response is insufficient to provide a good fit over the whole signal spectrum. It was then found that a third term having a lifetime of less than 100 fs was required to obtain a good fit.

Using Eq. (4.1), excellent fits were obtained for both positive and negative detuning data with the same parameter set (as shown in Figure 4.4 for the three term fit). The fitting parameters used in Figure 4.4 are as follows: $\tau_1 = 200$ ps, $\tau_2 = 650$ fs,

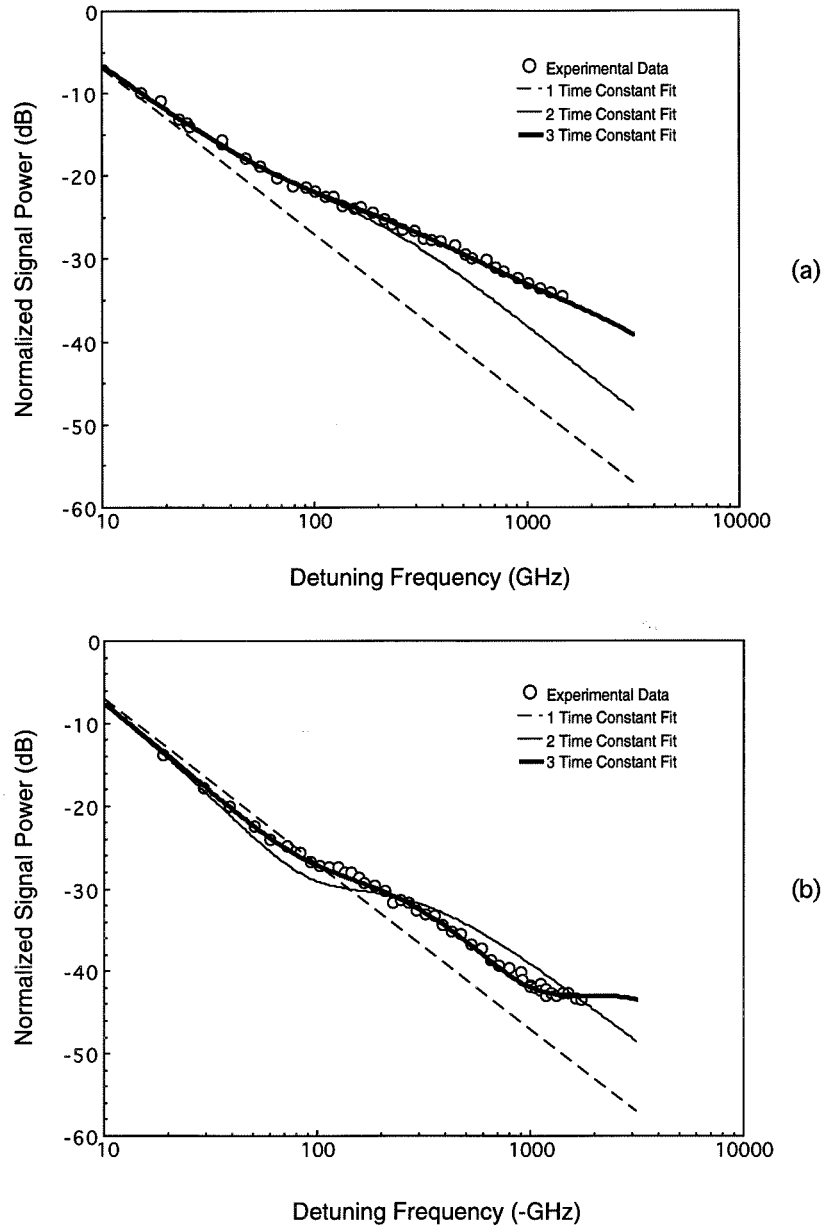

Figure 4.4: Normalized four-wave mixing signal power versus (a) positive and (b) negative detuning frequencies showing theoretical fits. The SOA measured was a tensile strained multiple quantum well amplifier.

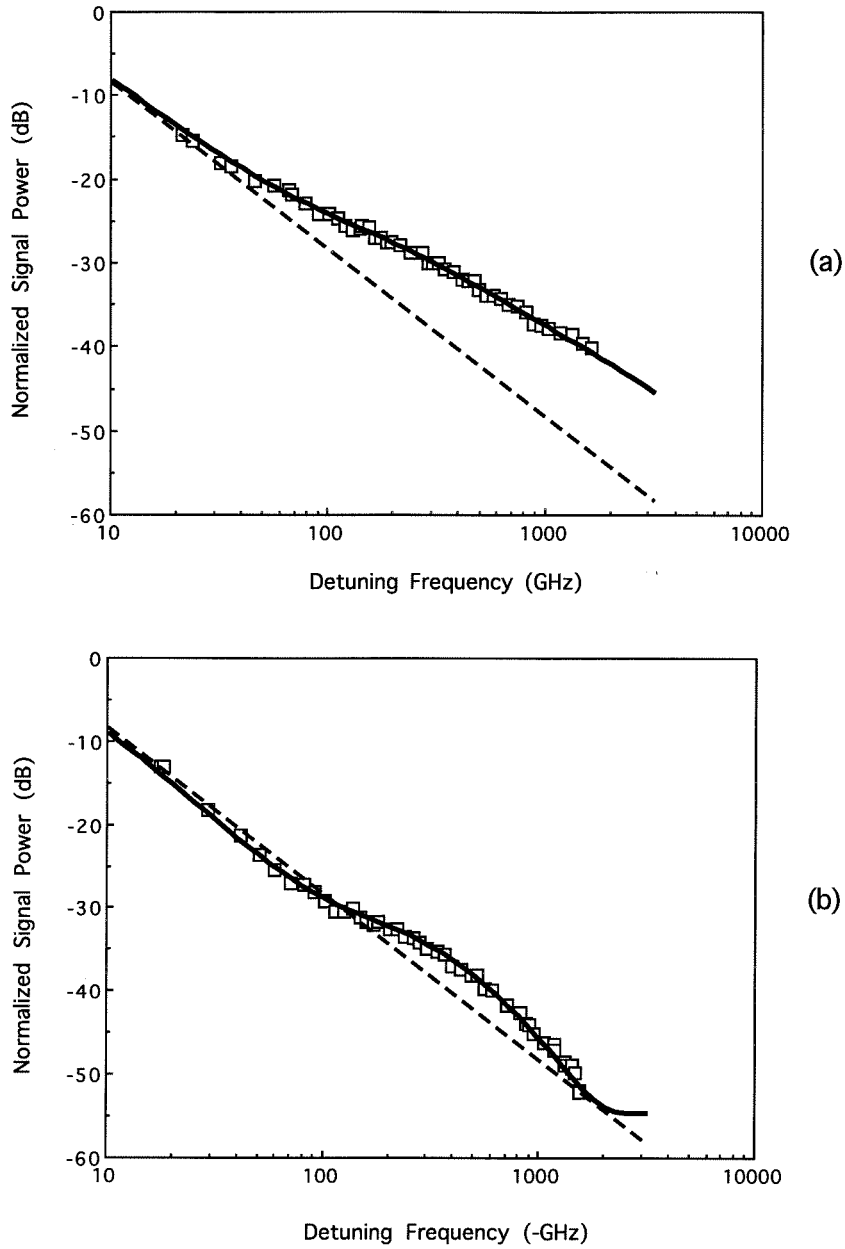

Figure 4.5: Normalized four-wave mixing signal power versus (a) positive and (b) negative detuning frequencies showing theoretical fits. The SOA measured was a compressively strained multiple quantum well amplifier.

$\tau_3 = 50$ fs, $C_1 = 0.24$, $C_2 = 0.0027e^{i2.60}$, $C_3 = 0.00048e^{i2.83}$. We note that there can be an arbitrary global phase factor in the complex coupling coefficients, as can be seen from Eq. (4.1).

The compressively-strained SOA data, shown in Figure 4.5, are also accompanied by theoretical fits using Eq. (4.1). The fits were obtained using the same relaxation time constants as for the tensile device, but using different complex coupling coefficients: $C_1 = 0.24$, $C_2 = 0.0027e^{i2.72}$, $C_3 = 0.00023e^{i4.43}$. Very good fits were obtained for both positive and negative detuning frequencies, as shown in Figure 4.5.

The time constant of 650 fs obtained in this study is in good agreement with the results of previous measurements of carrier heating in both time-domain [1] and frequency-domain [12],[13]. The time constant for the fastest intraband mechanism used in the fit is 50 fs. However, it is important to note that the fit is relatively insensitive to this parameter (empirically we can obtain good fits provided $\tau_3 < 100$ fs) because the time resolution, or equivalently, the detuning frequency, is still limited in the measurements. Therefore, this time constant and its associated C parameter used in the fit give somewhat qualitative information on the fastest mechanism. However, the fact that a third term, having a time constant of < 100 fs, is required to obtain a good fit clearly indicates the presence of additional ultrafast intraband processes. They are believed to be related to intraband carrier-carrier scattering, *i.e.*, spectral hole burning and the initial thermalization of carrier heating, as discussed in our theoretical analysis.

4.4 Conclusion

Since gain and index gratings both contribute to the four-wave mixing process, the interpretation of four-wave mixing experimental results is somewhat more complicated than in the case of time-domain measurements, where gain and index contributions can be separated [12],[13]. However, the different interference behaviors present in positive and negative detuning signal spectra considerably facilitate theoretical analysis of the experimental data in four-wave mixing. Furthermore, the measurement presents data in a form that is complementary to femtosecond studies, *i.e.*, frequency-domain rather than time-domain, and is inherently a small signal approach. This latter point may explain the good agreement we find between a simple model and our data.

Bibliography

[1] L. F. Tiemeijer, "Effects of nonlinear gain on four-wave mixing and asymmetric gain saturation in a semiconductor laser amplifier," *Appl. Phys. Lett.*, vol. 59, pp. 499–501, 1991.

[2] K. Kikuchi, M. Kakui, C. E. Zah, and T. P. Lee, "Observation of highly nondegenerate four-wave mixing in a 1.5 μm traveling-wave semiconductor optical amplifier and estimation of nonlinear gain coefficient," *IEEE J. Quantum Electron.*, vol. 28, pp. 151–156, 1992.

[3] J. Zhou, N. Park, J. W. Dawson, K. J. Vahala, M. A. Newkirk, U. Koren, and B. I. Miller, "Highly nondegenerate four-wave mixing and gain nonlinearity in a strained multiple-quantum-well optical amplifier," *Appl. Phys. Lett.*, vol. 62, pp. 2301–2303, 1993.

[4] J. Zhou, N. Park, J. W. Dawson, K. J. Vahala, M. A. Newkirk, and B. I. Miller, "Terahertz four-wave mixing spectroscopy for study of ultrafast dynamics in a semiconductor optical amplifier," *Appl. Phys. Lett.*, vol. 63, pp. 1179–1181, 1993.

[5] A. D'Ottavi, E. Iannone, A. Mecozzi, S. Scotti, P. Spano, J. Landreau, A. Ougazzaden, and J. C. Bouley, "Investigation of carrier heating and spectral hole burning in semiconductor amplifiers by highly nondegenerate four-wave mixing," *Appl. Phys. Lett.*, vol. 64, pp. 2492–2494, 1994.

[6] A. Uskov, J. Mørk, J. Mark, M. C. Tatham, and G. Sherlock, "Terahertz four-wave mixing in semiconductor optical amplifiers: experiment and theory," *Appl. Phys. Lett.*, vol. 65, pp. 944–946, 1994.

[7] J. Zhou, N. Park, K. J. Vahala, M. A. Newkirk, and B. I. Miller, "Study of inter-well carrier transport by terahertz four-wave mixing in an optical amplifier

with tensile and compressively strained quantum wells," *Appl. Phys. Lett.*, vol. 65, pp. 1897–1899, 1994.

[8] N. Park, J. W. Dawson, K. J. Vahala, and C. Miller, "All fiber, low threshold, widely tunable single-frequency, erbium-doped fiber ring laser with a tandem fiber Fabry-Perot filter," *Appl. Phys. Lett.*, vol. 59, pp. 2369–2371, 1991.

[9] N. Park, J. W. Dawson, and K. J. Vahala, "Linewidth and frequency jitter measurement of an erbium-doped fiber ring laser by a loss-compensated, delayed self-heterodyne interferometer," *Opt. Lett.*, vol. 17, pp. 1274–1276, 1992.

[10] B. I. Miller, U. Koren, M. A. Newkirk, M. G. Young, R. M. Jopson, R. M. Derosier and M. D. Chien, "Tensile-strained InGaAs/InGaAsP quantum-well optical amplifier with a wide spectral gain region at 1.55 μm," *IEEE Photon. Technol. Lett.*, vol. 5, pp. 520–522, 1993.

[11] M. A. Newkirk, U. Koren, B. I. Miller, M. D. Chien, M. G. Young, T. L. Koch, G. Raybon, C. A. Burrus, B. Tell, and K. F. Brown-Goebeler, "Three-section semiconductor optical amplifier for monitoring of optical gain," *IEEE Photon. Technol. Lett.*, vol. 4, pp. 1258–1260, 1992.

[12] K. L. Hall, J. Mark, E. P. Ippen, and G. Eisenstein, "Femtosecond gain dynamics in InGaAsP optical amplifiers," *Appl. Phys. Lett.*, vol. 56, pp. 1740–1742, 1990.

[13] K. L. Hall, G. Lenz, E. P. Ippen, U. Koren, and G. Raybon, "Carrier heating and spectral hole burning in strained-layer quantum-well laser amplifiers at 1.5 μm," *Appl. Phys. Lett.*, vol. 61, pp. 2512–2514, 1992.

Chapter 5

Inter-Well Carrier Transport Dynamics

5.1 Introduction

Carrier transport in quantum well lasers and amplifiers is a complicated and nonlinear process which has been shown to affect both the static and dynamic performance characteristics of these devices, including the maximum modulation bandwidth of quantum well lasers [1]. Shown in Figure 5.1 is the conceptual band diagrams of a bulk laser and a quantum well laser. In a bulk laser, carriers are injected directly into the gain region where they participate in the lasing process. Gain nonlinearities in bulk lasers are therefore essentially material dependent, through mechanisms such as carrier heating and spectral hole burning. In contrast, gain region in a quantum well laser is embedded in a large optical confinement region. To contribute to the optical gain, the injected carriers have to take an additional step, *i.e.*, reaching the

bottom of the wells, as illustrated in Figure 5.1. This results in a structure-dependent nonlinearity, often referred to as well-barrier hole burning [2].

Carriers in the well regions, confined in one dimension and having discrete energy bands, can be considered as two-dimensional (2-D) carriers. Carriers in the confinement and barrier regions could be treated quantum mechanically, for instance, by the wave packet formalism [3]. For simplicity, however, these carriers are often treated as three-dimensional (3-D) carriers whose transport is by diffusion and drift. The classical treatment has been supported by a number of experimental studies, such as photoluminescence [4], pump-probe [5],[6] and modulation response measurements [7],[8]. The overall carrier transport process can thus be considered to include capture and escape of carriers between unconfined 3-D and confined 2-D quantum states in the well regions, as well as diffusion and drift of 3-D carriers across the confinement region and between wells in the barrier regions. The overall carrier transport process is also conceptually illustrated in Figure 5.1. Since Rideout *et al.* [2] first proposed a well-barrier hole burning model, a number of theoretical and experimental investigations [4]–[11] have studied these processes.

As presented in the previous chapter, four-wave mixing in semiconductor traveling-wave amplifiers has in recent years been demonstrated as an important frequency-domain technique for study of carrier dynamics in semiconductor active layers [12]–[17]. In this chapter, we describe the first investigation of inter-well transport using a novel four-wave mixing technique that selectively excites and probes adjacent quantum wells according to strain, thereby studying inter-well carrier transport [18].

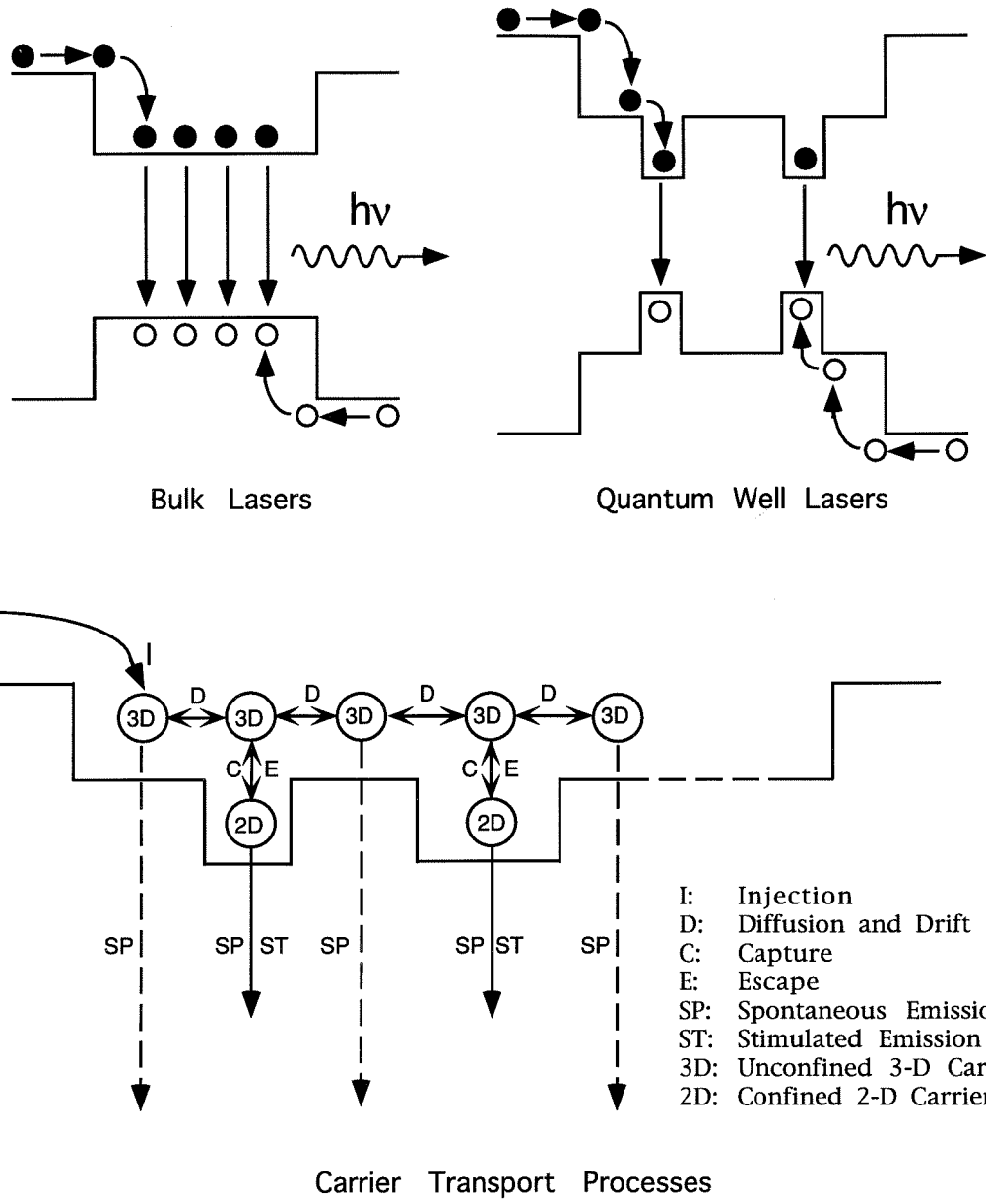

Figure 5.1: Upper figure shows the difference between bulk and quantum well lasers. Lower figure illustrates details of carrier transport in a multiple quantum well laser.

5.2 Cross-Polarized Four-Wave Mixing Experiments

The semiconductor optical amplifier (SOA) used in the measurement was an InGaAs/InGaAsP multiple quantum well traveling-wave amplifier operating at 1.5 μm [19]. The active layer contains six alternating-strain (tensile and compressive) InGaAs quantum wells. It is known that the tensile wells provide predominantly TM gain, while the compressive wells provide TE gain but have vanishing TM gain. The scheme of both tensile and compressively strained wells in the same active region was originally designed to eliminate the polarization sensitivity of the amplifier gain [19]. Indeed, the measured gain spectra indicate a gain insensitivity of less than 1 dB on the average over the amplifier gain bandwidth.

Similar to the amplifiers described in the previous chapter, the alternating-strain device was grown by atmospheric pressure MOVPE. As shown in Figure 5.2, the base wafer comprises the tensile/compressive gain layer on top of a 3200 Å thick InGaAsP passive waveguide. The quantum well stack is composed of three 35 Å thick InGaAs wells with 1.0% compressive strain and three 160 Å thick InGaAs wells with 1.0% tensile strain. The wells are alternately tensile and compressive, separated by a 100 Å thick lattice matched InGaAsP barrier ($E_g = 0.95$ eV). 620 μm long active sections were then defined by selective etching down to the waveguide layer. The device also used the semi-insulating planar buried-heterostructure configuration. 2.5 μm wide mesas were created by standard photolithography and wet chemical etching, followed by two MOVPE regrowths for current blocking, cladding and p-type contacting layers. The passive waveguide extends 15 μm beyond the active section at each end. To

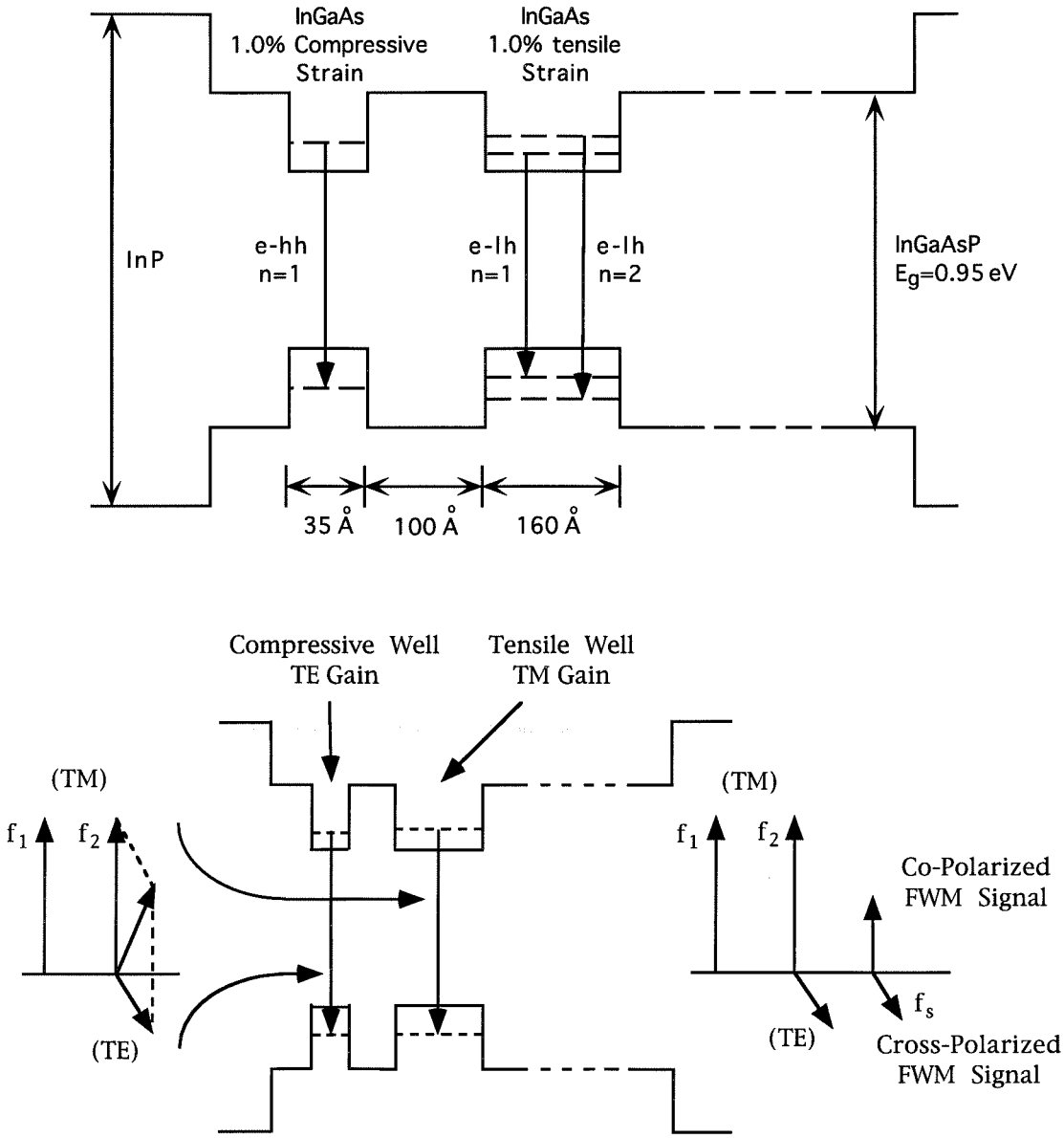

Figure 5.2: Upper figure shows the band diagram of the amplifier having alternative tensile and compressively strained InGaAs quantum wells. The lower figure illustrates co- and cross-polarized four-wave mixing processes.

minimize reflections from the cleaved facets, the passive waveguide was terminated to form a 35 μm long window at the input and output. The facets were also antireflection coated with a single SiO layer to achieve modal reflectivity $< 1 \times 10^{-4}$. At a bias current of 150 mA, the amplifier was measured to have an optical gain of about 14.5 dB at 1.55 μm for both the TE and TM polarizations.

We made use of this special device structure to selectively excite and probe adjacent wells according to polarization. As illustrated in Figure 5.2, input beam 1, having optical frequency f_1 and a given polarization (either TE or TM), and input beam 2, having optical frequency f_2 and a polarization at an angle of 45 degrees with respect to beam 1, were coupled into the SOA. For the configuration shown in Figure 5.2, beating of the TM-polarized beam 1 and the TM component of beam 2 excites carriers in the tensile wells through interband transitions. As a result, a TM-polarized four-wave mixing signal at $2f_2 - f_1$ was generated. This conventional four-wave mixing is referred here as co-polarized four-wave mixing. On the other hand, while carriers in the compressively strained wells do not experience the optical beating because of the polarization selection rule, the excited carriers in the tensile well regions can be transported to the neighboring compressive wells. The TE-polarized component of beam 2 then probes this transported carrier dynamic in the compressive wells, leading to the generation of a TE-polarized four-wave mixing signal also at $2f_2 - f_1$. We refer to this process as cross-polarized four-wave mixing. Since the cross-polarized four-wave mixing process involves inter-well carrier transport, the observed difference between the co- and cross-polarized signal spectra gives information about inter-well carrier

transport. Measurements of co- and cross-polarized four-wave mixing can therefore be used as a frequency-domain tool for analysis of the inter-well transport processes.

The experimental arrangement for this study was similar to what we have described in the previous chapter except here the input beams were combined using a beam splitter to allow independent polarization control. The co- and cross-polarized four-wave mixing signals were measured using the same heterodyne detection system as shown in Figure 4.3 in which the SOA output, after passing a polarizer (selecting TE or TM polarization), was mixed with a tunable fiber laser local oscillator. Using this experimental setup, we carried out co- and cross-polarized four-wave mixing measurements in which either the tensile wells were selectively excited with TM-polarized pumps, or the compressive wells were selectively excited with TE-polarized pumps. Figure 5.3 shows the measured four-wave mixing signal powers, normalized by the pump and probe amplitudes, plotted versus the detuning frequency $f_2 - f_1$ up to 1 THz for various pump-probe polarization configurations.

5.3 Analysis of Experimental Results

As shown in previous conventional four-wave mixing studies [12]–[17], contributing mechanisms to four-wave mixing are interband carrier number modulation and intraband occupancy modulation. The former is characterized by the interband carrier lifetime which is on the order of several hundred picoseconds in quantum well amplifier devices. The latter typically includes dynamic carrier heating and spectral hole burning. For the detuning frequencies measured in this measurement (up to 1 THz),

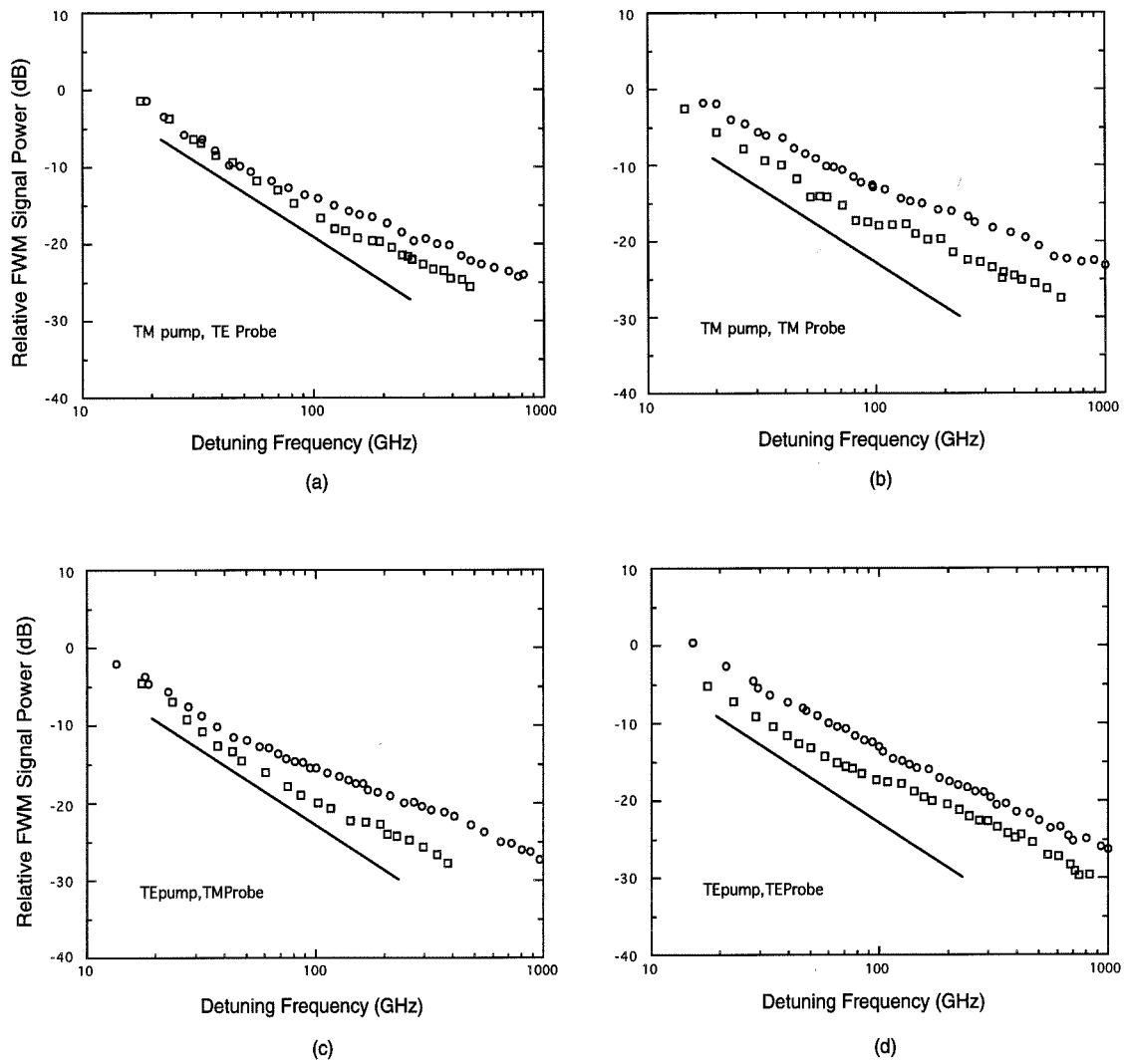

Figure 5.3: Normalized four-wave mixing signal power versus positive (○) and negative (□) detuning frequencies for various pump-probe polarization configurations: (a) TM pump, TE probe; (b) TM pump, TM probe; (c) TE pump, TM probe; (d) TE pump, TE probe.

four-wave mixing is dominated by carrier number modulation and carrier temperature modulation, *i.e.*, the first two terms in Eq. (4.1) provide dominant contributions to the four-wave mixing signal.

The cross-polarized four-wave mixing signal spectra, as shown in Figures 5.3(a) and 5.3(c), are symmetrical at low frequencies with respect to positive and negative detuning, in contrast to the co-polarized signal spectra which exhibit a steady asymmetry, as shown in Figures 5.3(b) and 5.3(d). Since this asymmetry results from signal phase interferences between the contributing four-wave mixing mechanisms, namely, carrier number modulation and carrier temperature modulation in this study, the difference between the co- and cross-polarized four-wave mixing signal spectra indicates that phase interferences are stronger in the case of co-polarized four-wave mixing versus the case of cross-polarized four-wave mixing. This suggests that carrier number modulation and carrier temperature modulation experience different transport efficiencies.

The inter-well carrier number transport can be approximately described as a three-step process, as shown in Figure 5.1. First, 2-D carriers in the excited well are coupled to the 3-D states in the same well through quantum capture/escape processes. These 3-D carriers are then transported to the nonexcited wells through the combined effect of diffusion and drift. Finally, also through carrier capture/escape processes, the transported 3-D carriers fall into the 2-D states in the nonexcited well, where they contribute to the cross-polarized four-wave mixing signal. For carrier temperature modulation, in addition to the above-mentioned processes, carrier-carrier scattering

can also assist the temperature transport.

During the inter-well transport process, the two modulations (carrier number and temperature) experience different damping mechanisms, *i.e.*, transport of carrier number modulation is damped by spontaneous interband carrier recombination, while the carrier temperature modulation is damped by carrier-lattice interactions having a much shorter relaxation time. These widely different damping rates can considerably affect the corresponding inter-well transport efficiencies.

To illustrate, we calculate the trans-barrier transport efficiency by considering 3-D carrier transport from an excited well to the adjacent nonexcited well using a simple one-dimensional (1-D) diffusion equation

$$\frac{\partial W}{\partial t} = D\frac{\partial^2 W}{\partial y^2} - \frac{W}{\tau} \tag{5.1}$$

where W represents either carrier number or temperature. D and τ are the diffusion constant and lifetime associated with the respective modulations. The modulation at the excited well ($y = 0$) is given by $W = W_0 \exp(-i\Omega t)$, where $\Omega/2\pi$ is the detuning frequency. The solution to Eq. (5.1) is found to be

$$W(y,t) = W_0 \exp\left(-\frac{y}{\sqrt{D}}\sqrt{\frac{1}{\tau} - i\Omega} - i\Omega t\right) \tag{5.2}$$

The trans-barrier transport efficiency is then given by

$$\zeta = \exp\left(-\frac{s}{\sqrt{D}}\sqrt{\frac{1}{\tau} - i\Omega}\right) \tag{5.3}$$

where s is the separation between adjacent wells.

Since the carrier number damping time ($\sim$ 1 ns) is much longer than the temperature damping time ($\sim$ 1 ps), carrier temperature modulation transport is much

less efficient than carrier number transport, particularly at low detuning frequencies. Here we have assumed comparable diffusion constants for the two modulations in the above discussion. Another contributing mechanism to the trans-barrier transport is drift of 3-D carriers caused by internal fields. The drift process, like the diffusion process, also favors the mechanism having the longer time constant so that, assuming all other factors are comparable, carrier number transport is again expected to be more efficient than the carrier temperature transport.

Similarly, the efficiency associated with the escape/capture dynamics are also subject to the damping effect. Widely different relaxation time constants for the two modulations should lead to very different efficiencies in the escape/capture process. We would therefore expect overall inter-well transport to exhibit a higher efficiency for the carrier number modulation than for the temperature modulation. Consequently, phase interferences are suppressed in the cross-polarized measurement, causing the highly symmetrical spectra. This qualitatively explains the observed difference between the co- and cross-polarized spectra shown in Figure 5.3.

The co- and cross-polarized four-wave mixing signals, as shown in Figure 5.3, exhibit comparable amplitudes at low frequencies. Furthermore, the cross-polarized four-wave mixing data in Figures 5.3(a) and (c) do not show any roll-off induced by the carrier number transport, *i.e.*, beyond the 20 dB/decade roll-off caused by the interband modulation within the excited wells. This indicates that carrier number modulation, which is responsible for the low frequency data, is coupled from excited wells to nonexcited wells with little loss. This agrees qualitatively with a calculation

of the trans-barrier transport efficiency function which gives $|\zeta| > 78\%$ for $\tau = 1$ ns, $D = 5$ cm^{2}s^{-1}, $s = 100$ Å and $\Omega/2\pi < 100$ GHz. The data measured in this study also suggest that the inter-well carrier number transport in the present device is fast enough so that carrier number modulation in nonexcited wells behaves as if it were generated within these wells for frequencies at least as high as 100 GHz. Beyond this frequency the modulation data is obscured by the presence of additional mechanisms, making prediction of a definitive upper transport rate impossible.

It should be mentioned that carrier heating induced by free-carrier absorption is not strain selective. Specifically, it can take place in both types of wells when pumps are TE-polarized, but it is inhibited in all wells when pumps are TM-polarized due to the quantum well confinement barrier. Therefore, temperature modulation within the nonexcited wells is potentially significant in the case of TE pumps. This might explain the observed difference in the two sets of cross-polarized spectra at low detuning frequencies, where data with TE pumps show an earlier onset of reduced symmetry, *i.e.*, more phase interference between carrier number and temperature modulations.

5.4 Conclusion

We have presented in this chapter the measurements of co- and cross-polarized four-wave mixing up to 1 THz in a SOA having alternating tensile and compressively strained quantum wells. The effect of inter-well carrier transport on four-wave mixing signal spectra is observed and an explanation is provided by noting the different transport efficiencies for carrier number and temperature modulations. A lower bound

of inter-well carrier number transport of 100 GHz is estimated by analyzing the measured data. It is important, however, to point out that the complexities of this system require a more sophisticated theoretical treatment.

Bibliography

[1] G. P. Agrawal and G. R. Gray, "Importance of nonlinear gain in semiconductor lasers," *SPIE Proc.*, vol. 1497, pp. 444–455, 1991.

[2] W. Rideout, W. F. Sharfin, E. S. Koteles, M. O. Vassell, and B. Elman, "Well-barrier hole burning in quantum well lasers," *IEEE Photon. Technol. Lett.*, vol. 3, 784–786, 1991.

[3] K. J. Vahala and A. Yariv, "Application of wave packet formalism to local equations of motion for semiconductor lasers," *Phys. Rev. B*, vol. 32, pp. 345–356, 1985.

[4] S. Morin, B. Deveaud, F. Clerot, K. Fujiwara, and K. Mitsunaga, "Capture of photoexcited carriers in a single quantum well with different confinement structure," *IEEE J. Quantum Electron.*, vol. 27, pp. 1669–1675, 1991.

[5] G. Eisenstein, J. M. Wiesenfeld, M. Wegener, G. Sucha, D. S. Chemla, S. Weiss, G. Raybon, and U. Koren, "Ultrafast gain dynamics in 1.5 μm multiple quantum well optical amplifiers," *Appl. Phys. Lett.*, vol. 58, 158–160, 1991.

[6] S. Weiss, J. M. Wiesenfeld, D. S. Chemla, G. Raybon, G. Sucha, M. Wegener, G. Eisenstein, C. A. Burrus, A. G. Dentai, U. Koren, B. I. Miller, H. Temkin, R. A. Logan, and T. Tanbun-Ek, "Carrier capture times in 1.5 μm multiple quantum well optical amplifiers," *Appl. Phys. Lett.*, vol. 60, pp. 9–11, 1992.

[7] R. Nagarajan, M. Ishikawa, T. Fukushima, R. S. Geels, and J. E. Bowers, "High speed quantum-well lasers and carrier transport effects," *IEEE J. Quantum Electron.*, vol. 28, pp. 1990–2007, 1992.

[8] M. Ishikawa, R. Nagarajan, T. Fukushima, J. G. Wasserbauer, and J. E. Bowers, "Long wavelength high-speed semiconductor lasers with carrier transport effects," *IEEE J. Quantum Electron.*, vol. 28, pp. 2230–2241, 1992.

[9] S. C. Kan, D. Vassilovski, T. C. Wu, and K. Y. Lau, "On the effects of carrier diffusion and quantum capture in high speed modulation of quantum well lasers," *Appl. Phys. Lett.*, vol. 61, pp. 752–754, 1992.

[10] S. C. Kan, D. Vassilovski, T. C. Wu, and K. Y. Lau, "Quantum capture limited modulation bandwidth of quantum well, wire, and dot lasers," *Appl. Phys. Lett.*, vol. 62, pp. 2307–2309, 1993.

[11] N. Tessler and E. Eisenstein, "On carrier injection and gain dynamics in quantum well lasers," *IEEE J. Quantum Electron.*, vol. 29, pp. 1586–1595, 1993.

[12] L. F. Tiemeijer, "Effects of nonlinear gain on four-wave mixing and asymmetric gain saturation in a semiconductor laser amplifier," *Appl. Phys. Lett.*, vol. 59, pp. 499–501, 1991.

[13] K. Kikuchi, M. Kakui, C. E. Zah, and T. P. Lee, "Observation of highly nondegenerate four-wave mixing in a 1.5 μm traveling-wave semiconductor optical amplifier and estimation of nonlinear gain coefficient," *IEEE J. Quantum Electron.*, vol. 28, pp. 151–156, 1992.

[14] J. Zhou, N. Park, J. W. Dawson, K. J. Vahala, M. A. Newkirk, U. Koren, and B. I. Miller, "Highly nondegenerate four-wave mixing and gain nonlinearity in a strained multiple-quantum-well optical amplifier," *Appl. Phys. Lett.*, vol. 62, pp. 2301–2303, 1993.

[15] J. Zhou, N. Park, J. W. Dawson, K. J. Vahala, M. A. Newkirk, and B. I. Miller, "Terahertz four-wave mixing spectroscopy for study of ultrafast dynamics in a semiconductor optical amplifier," *Appl. Phys. Lett.*, vol. 63, pp. 1179–1181, 1993.

[16] A. D'Ottavi, E. Iannone, A. Mecozzi, S. Scotti, P. Spano, J. Landreau, A. Ougazzaden, and J. C. Bouley, "Investigation of carrier heating and spectral hole burning in semiconductor amplifiers by highly nondegenerate four-wave mixing," *Appl. Phys. Lett.*, vol. 64, pp. 2492–2494, 1994.

[17] A. Uskov, J. Mørk, J. Mark, M. C. Tatham, and G. Sherlock, "Terahertz four-wave mixing in semiconductor optical amplifiers: experiment and theory," *Appl. Phys. Lett.*, vol. 65, pp. 944–946, 1994.

[18] J. Zhou, N. Park, K. J. Vahala, M. A. Newkirk, and B. I. Miller, "Study of inter-well carrier transport by terahertz four-wave mixing in an optical amplifier with tensile and compressively strained quantum wells," *Appl. Phys. Lett.*, vol. 65, pp. 1897–1899, 1994.

[19] M. A. Newkirk, B. I. Miller, U. Koren, M. G. Young, M. Chen, R. M. Jopson, and C. A. Burrus, "1.5 μm multi-quantum-well semiconductor optical amplifier with tensile and compressively strained wells for polarization-independent gain," *IEEE Photon. Technol. Lett.*, vol. 5, pp. 406–408, 1993.

Chapter 6

Broadband Four-Wave Mixing Wavelength Conversion

6.1 Introduction

6.1.1 Fiber-Optic Communications

A communication system transmits information from one place to another, whether separated by a few kilometers or by transoceanic distances. If information is carried by an electromagnetic wave in the optical spectrum (carrier frequency $\sim$ 100 THz), such communication systems are called lightwave systems to distinguish from microwave systems whose carrier frequency is typically smaller by five orders of magnitude ($\sim$ 1 GHz). Fiber-optic communication systems are lightwave systems that employ optical fibers as the transmission medium.

The key idea for optical fiber communications was proposed in 1966 in a publica-

tion by Charles K. Kao [1]. In that paper he noted that pure optical fiber was theoretically capable of guiding a light signal with very little loss. By 1970, loss of optical fiber was reduced to about 20 dB/km [2]. At about the same time, GaAs semiconductor diode lasers, operating continuously at room temperature, were demonstrated [3]. The simultaneous availability of a compact optical source and low-loss transmission media lead to a worldwide effort for developing fiber-optic communication systems.

The technologies required for fiber-optic communications have progressed since then at an extremely rapid pace [4],[5]. These technological advances and market demand for cost-effective transmission of large amounts of information have propelled fiber-optic systems from laboratory research to widespread field deployment. Fiber-optic transmission systems are now employed in virtually all areas of telecommunications [6]: undersea cables spanning oceans, terrestrial long-haul networks connecting cities, trunk lines that shuttle traffic between switching offices in metropolitan areas, and subscriber loop systems that serve customer premises. More recently, the cable-television industry has begun deploying fibers for trunking and distribution, and optical fiber local area networks have been installed for computer networking.

Research continues today on many fronts to explore more efficient use of the ultra-broad bandwidth of optical fibers for long-haul transport, high-throughput computer networking and distribution of broadband services. Two distinctive efforts have been pursued to increase transmission capacity per optical fiber: one is higher speed serial transmission or time-division-multiplexing (TDM), and the other is paralleled transmission of multiple channels at different wavelengths or wavelength-division-

multiplexing (WDM). The former approach used to be favored since the cost of a single high-speed optoelectronic regenerator is generally less than that of several low speed regenerators and a pair of demultiplexer and multiplexer. Although the speeds of electronic circuits continue to advance and optical TDM techniques are being actively explored, it is highly unlikely that the tens of THz of available fiber bandwidth can be spanned by TDM technologies alone. Thus, WDM will be ultimately required.

The advent of Erbium-doped fiber amplifiers (EDFA's) has hastened the move to WDM. EDFA's can amplify WDM signals without the need for demultiplexing and optoelectronic regenerating the individual channels as in conventional fiber-optic systems. This simple and elegant function, which is independent of operating data rate, has greatly accelerated the pace at which high capacity WDM lightwave systems are being developed. For example, in a recent WDM transmission experiment, 40 Gb/s was sent through a 1420-km-long fiber using 16 channels of 2.5 Gb/s each, with EDFA spacings ranging from 96 km to 123 km [7]. More recently, a record-breaking 340 Gb/s was transmitted over 150 km as 17 WDM channels of 20 Gb/s each, with EDFA's spaced every 50 km [8].

6.1.2 All-Optical Network and Wavelength Conversion

WDM multiwavelength transmission not only increases aggregate network capacity, it is also attractive for networking applications where wavelength selective devices may be used for circuit access and routing. The latter point also represents the basis for the all-optical networking that is being actively explored by researchers worldwide under various consortia [9],[10]. In these all-optical networks, some of the network routing

functions are all-optical, making geographical distribution of switching functions more flexible.

Early multiwavelength all-optical networks were designed around a broadcast-and-select concept, where all users were connected to a "passive optical broadcast star." The central problem in broadcast networks is that all wavelengths share the same transmission paths. This forces the number of wavelengths to be continually increased as new users are added to the network. While these passively routed broadcast networks can be appropriate for local-area networks (LAN's), they are not suitable for larger scale networks due to the limited number of wavelengths available.

Large networks can be built by interconnecting many LAN's based on wavelength conversion and wavelength routing, with the same set of wavelengths used in each LAN's [9],[10]. Routing between LAN's can be accomplished by shifting one of the wavelengths from the incoming LAN, using a broadband wavelength converter, so that it can be routed to the desired recipient LAN. This architecture makes it possible to build multiwavelength networks in which the number of nodes is completely independent of the number of wavelengths. Such networks are truly scalable and overcome the limitations placed on broadcast networks by the limited number of wavelengths available. In addition, wavelength conversion, combined with wavelength routing, makes it possible to dynamically reconfigure the connection paths in an all-optical network. This can potentially enhance network survivability, a network quality highly sought after by service providers.

Because of their potential applications in all-optical networks, wavelength con-

version devices have been extensively investigated in recent years. Demonstrations to date of wavelength converters include: optical triggering in distribution-feedback (DFB) lasers with saturable absorbers [11]; gain saturation in semiconductor optical amplifiers (SOA's) [12] and semiconductor lasers [13]; difference frequency generation in $LiNbO_3$ channel waveguides [14]; and four-wave mixing in dispersion-shifted fibers [15], semiconductor lasers [16] and traveling-wave amplifiers [17]–[20]. Various limitations with respect to tuning and modulation format are inherent with most of these wavelength conversion techniques. However, wavelength conversion based on four-wave mixing in SOA's allows continuous tuning of input and output wavelengths over the entire amplifier gain bandwidth, and the process is transparent to the modulation format and bit-rate of the data.

In this chapter we present our results concerning conversion efficiency over wavelength spans up to 65 nm [18], as well as a demonstration of wavelength conversion with gain [20]. We also describe measurements of the signal to background noise ratio and present a noise reduction technique using a selective noise filter [21]. In addition, we describe a demonstration of wavelength conversion of modulated signals at data rates of 2.5 Gb/s and 10 Gb/s.

6.2 Wavelength Conversion Efficiency

Using Eq. (4.1), SOA four-wave mixing wavelength conversion efficiency can be expressed by the following simple relation:

$$\eta = 3G + 2I_p + R(\Delta\lambda) \tag{6.1}$$

where η is the ratio in dB of the converted signal output power to the signal input power in dBm and G is the saturated SOA optical gain in dB. Other parameters appearing in Eq. (6.1) include the input optical pump-wave power I_p (expressed in dBm), and a quantity we call the relative efficiency function, $R(\Delta\lambda)$, which is given by

$$R(\Delta\lambda) = 20\log|\sum_{m=1}^{3} c_m \cdot \frac{1}{1 - i2\pi f\tau_m}| \tag{6.2}$$

where, as discussed earlier, the three terms in the summation represent contributions to four-wave mixing wavelength conversion from the various responsible mechanisms. $\Delta\lambda$ is the wavelength shift related to detuning frequency by $\Delta\lambda = -2\lambda^2 f/c$.

A crucial point is the presence of $3G$ in this expression. This term occurs because the nonlinear field mixing involved in the four-wave mixing process uses the pump wave twice and the input signal once so that overall the amplifier's single-pass gain acts three times. As an aside, we note that $3G$ in Eq. (6.1) assumes equal gain for pump and signal waves. In general, we have $2G_{\text{pump}} + G_{\text{input}}$ where G_{pump} and G_{input} are pump and input signal gains, respectively.

In the present measurement, we employed a novel tandem amplifier geometry in which two or three 1.5 μm tensile-strained InGaAs/InGaAsP MQW SOA's [22] (the same devices used in the spectroscopy study), separated by optical isolators, were placed in series. This tandem amplifier, having much higher optical gain, provided a simple method for realizing higher optical gains and testing theoretical predictions concerning conversion efficiency.

We first measured the dependence of the conversion efficiency η on the saturated

single-pass SOA gain G. The experimental setup was similar to what we described in Chapter 4 except here a tandem amplifier with two SOA's was employed. For this measurement, wavelengths and powers of the pump and signal waves remained fixed, and the single-pass gain was varied by changing the bias currents of the two SOA's between 80 mA and 175 mA. Shown in Figure 6.1 is typical conversion efficiency data plotted versus single-pass saturated optical gain. Conversion was measured from 1532.0 nm to 1523.0 nm with a pump power of -5.2 dBm and an input signal power of -11.3 dBm. The measured slope of 3.18 verified the cubic dependence of efficiency on single-pass gain. Similar values for the slope were obtained for various other wavelength shifts and input power levels.

The wavelength-shift dependence of the conversion process was also measured for both wavelength up- and down-conversion. Both SOA's used in the measurements were biased at 150 mA. In the down-conversion experiment, the pump was fixed at 1526.0 nm with -5.3 dBm of power coupled into the first SOA wavelength converter. The maximum wavelength down-shift measured in this study was as large as 65 nm, corresponding to a frequency shift of 8 THz. In the up-conversion measurement, the pump was fixed at 1549.0 nm with an input power of -6.0 dBm. Wavelength up-conversion was measured for shifts up to 47.5 nm, corresponding to a frequency shift of -6 THz. The conversion efficiency η for both positive and negative wavelength shifts is presented in Figure 6.1, where the efficiency is normalized using Eq. (6.1) with the typical parameter values in this study: pump power of -5.5 dBm, signal power of -10 dBm and saturated optical gain G of 18.2 dB (corresponding to the

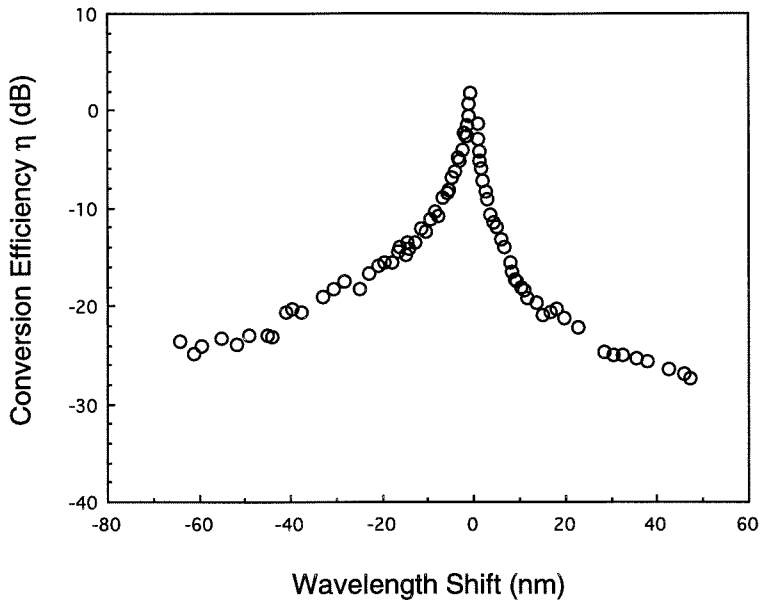

(a)

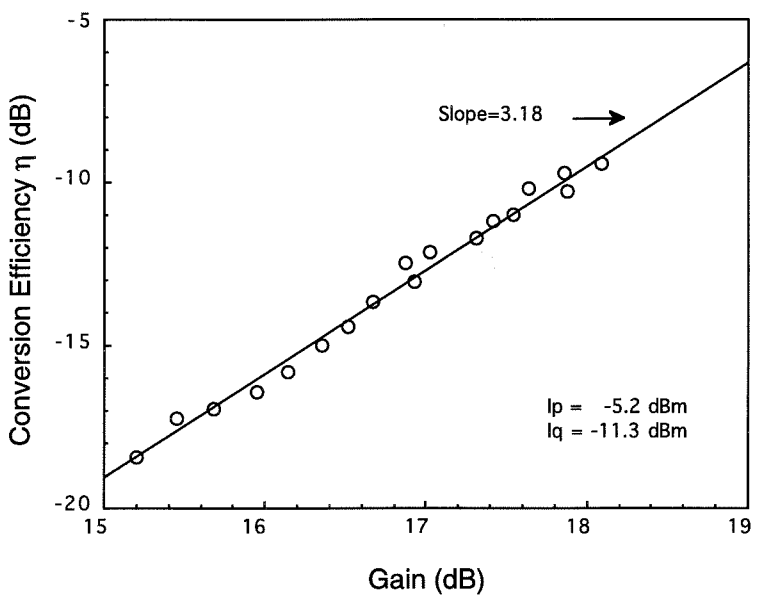

(b)

Figure 6.1: Measured conversion efficiency η (a) versus wavelength shift $\Delta\lambda$, (b) versus tandem amplifier gain G, showing the cubic dependence. A tandem amplifier with two tensile strained SOA's was used.

total input power). The normalization may introduce a small, but negligible error arising from slight spectral variation in the saturated SOA gain for the pump and input signal over the wavelength spans measured. An efficiency asymmetry with respect to positive and negative wavelength shifts is caused by phase interferences which occur between the various contributing inter- and intraband four-wave mixing mechanisms. The measurement of wavelength conversion up to 65 nm shows that ultrafast four-wave mixing dynamics in SOA's are capable of converting signals over very large wavelength spans.

In a separate measurement where three SOA's were used, we achieved $\eta > 0$ dB, *i.e.*, wavelength conversion with gain. The measured conversion efficiencies versus wavelength shift are presented in Figure 6.2 for a pump power of -11.5 dBm and a signal power of -15.2 dBm (SOA optical gain G was saturated to 24.2 dB at this input power level). Conversion efficiencies greater than 0 dB, as shown in Figure 6.2, were achieved for down-conversion up to ~ 7.0 nm and for up-conversion over ~ 2.0 nm. Conversion efficiency remained as high as 14% for down-conversion shifts as large as 23.9 nm. This was the first demonstration of broadband SOA four-wave mixing wavelength conversion with gain, indicating high conversion efficiency is possible with SOA four-wave mixing wavelength converters. In addition, we also confirmed the cubic dependence of conversion efficiency on the single-pass gain, as also shown in Figure 6.2.

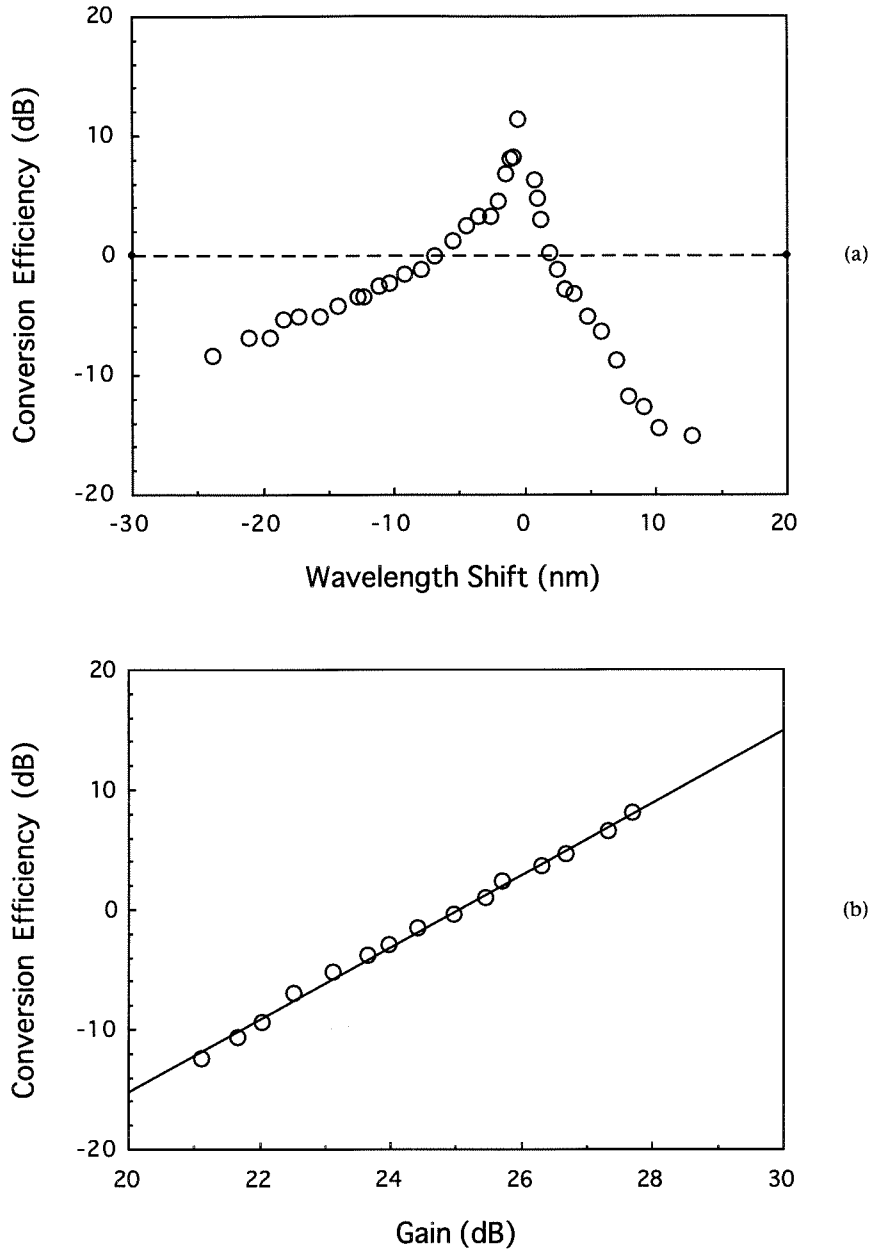

Figure 6.2: Measured conversion efficiency η (a) versus wavelength shift $\Delta\lambda$, (b) versus tandem amplifier gain G, showing the cubic dependence. A tandem amplifier with three tensile strained SOA's was used.

6.3 Noise Properties and Noise Reduction

6.3.1 Noise Properties

In SOA four-wave mixing wavelength conversion demonstrations to date, either the input signal is preamplified by an EDFA before being coupled into the SOA mixer [17],[19], or, as described in the previous section, a tandem SOA structure which provides high single-pass gain is used [18],[20]. In the latter case, the first SOA essentially serves as a preamplifier since the nonlinear mixing takes place primarily in the last segment of the tandem amplifier where the pump and input signal fields are strongest. The preamplification which occurs in each of these approaches is crucial to improving overall converter performance.

For a preamplifier having linear optical gain G_p and spontaneous emission factor n_{sp}^p, at the preamplifier output, the spontaneous noise power spectral density for one polarization state is given by

$$S_{out}^p(\nu) = G_p S_{in}^p(\nu) + n_{sp}^p \left(G_p - 1 \right) h\nu \tag{6.3}$$

where $S_{in}^p(\nu)$ is the spontaneous noise power spectral density at the preamplifier's input and $h\nu$ is photon energy. The two terms in the above formula originate from amplification of any input excess noise and introduction of spontaneous noise by the preamplifier. Assuming a coupling efficiency of κ_m to the SOA mixer, the spontaneous noise coupled to the mixer is given by $S_{in}^m = \kappa_m S_{out}^p$.

The spontaneous noise power spectral density of one polarization at the mixer's

output can be written as

$$S^m_{out}(\nu) = G_m S^m_{in}(\nu) + \eta_m(\Delta\nu) S^m_{in}(\nu - \Delta\nu) + n^m_{sp}\left(G_m - 1\right) h\nu \qquad (6.4)$$

where G_m and n^m_{sp} are the SOA's saturated single pass linear gain and spontaneous emission factor, respectively; $\eta_m(\Delta\nu)$ is the conversion efficiency of the SOA mixer for frequency shift $\Delta\nu$, defined as the ratio of converted signal power at the mixer's output to input signal power coupled into the mixer. Physically, the three terms on the right side in Eq. (6.4) represent amplified input excess noise, converted input noise, and spontaneous noise introduced by the SOA mixer, respectively.

Normally, a narrowband optical bandpass filter is used at the SOA mixer's output to remove the amplified pump and input signal, leaving only the converted signal. Upon detection of the converted signal, the photocurrent can be written as $I = I_{sig} + i$, where $I_{sig} = \kappa_d R P^{out}_m(\nu_{cs})$ is the signal and i represents current fluctuations which include the effects of shot noise, thermal noise and spontaneous noise. Here, κ_d is the coupling efficiency from the mixer's output to the detector, R is the detector's responsivity and $P^m_{out}(\nu_{cs})$ is the power of the converted signal (at optical frequency ν_{cs}) at the mixer's output. Under most circumstances the variance $\sigma^2 = \langle i^2 \rangle$ of current fluctuations is dominated by signal–spontaneous beat noise in which case the total current fluctuation $\langle i^2 \rangle$ is given by

$$\langle i^2 \rangle \approx \sigma^2_{sp-sig} = 4\kappa_d^2 R^2 P^m_{out}(\nu_{cs}) S^m_{out}(\nu_{cs}) \Delta f_{el} \qquad (6.5)$$

where Δf_{el} is the receiver's electrical bandwidth. Signal to noise ratio (SNR) can

therefore be given by

$$\mathrm{SNR} = \frac{\langle I \rangle^2}{\sigma^2} \approx \frac{\left(\kappa_d R P^m_{out}(\nu_{cs})\right)^2}{4\kappa_d^2 R^2 P^m_{out}(\nu_{cs}) S^m_{out}(\nu_{cs}) \Delta f_{el}} = \frac{P^m_{out}(\nu_{cs})}{4 S^m_{out}(\nu_{cs}) \Delta f_{el}} \tag{6.6}$$

As Eq. (6.6) indicates, optical SNR $\frac{P^m_{out}(\nu_{cs})}{S^m_{out}(\nu_{cs})\Delta f_{op}}$ (Δf_{op} is the normalization optical bandwidth), *i.e.*, the ratio of converted signal to background spontaneous noise in the converted signal band, is an important parameter for a wavelength converter. It directly affects the electrical SNR at the receiver, which in turn affects the bit-error-rate (BER) performance of a lightwave communication system. In the first experiment that we described in Section 6.2 where the tandem amplifier with two SOA's was used, optical SNR ($\Delta f_{op} = 0.1$ nm) for a total input power level of -4.2 dBm (as used in Figure 6.1) was measured to be about 15 dB for -5 nm of shift and steadily dropped to 0 dB slightly beyond -65 nm of shift.

Improvement in the optical SNR can be expected with higher total input power (pump plus input signal) because optical SNR increases with the total input power. Shown in Figure 6.3 is measured converted signal power, spontaneous noise power ($\Delta f_{op} = 0.1$ nm), and optical SNR as a function of total input power for a 5 nm wavelength down shift. The maximum optical SNR is 20.8 dB for -0.7 dBm of total input power. It results because of reduction of spontaneous noise in conjunction with increasing converted signal power as the amplifier saturates. As the total input power increases, both G_p and G_m are reduced as the result of gain saturation; therefore, the spontaneous noise at the mixer output decreases. The fact that converted signal power continues to increase in this regime is due to its cubic dependence on total output power at a fixed pump to signal power ratio, as indicated by the following

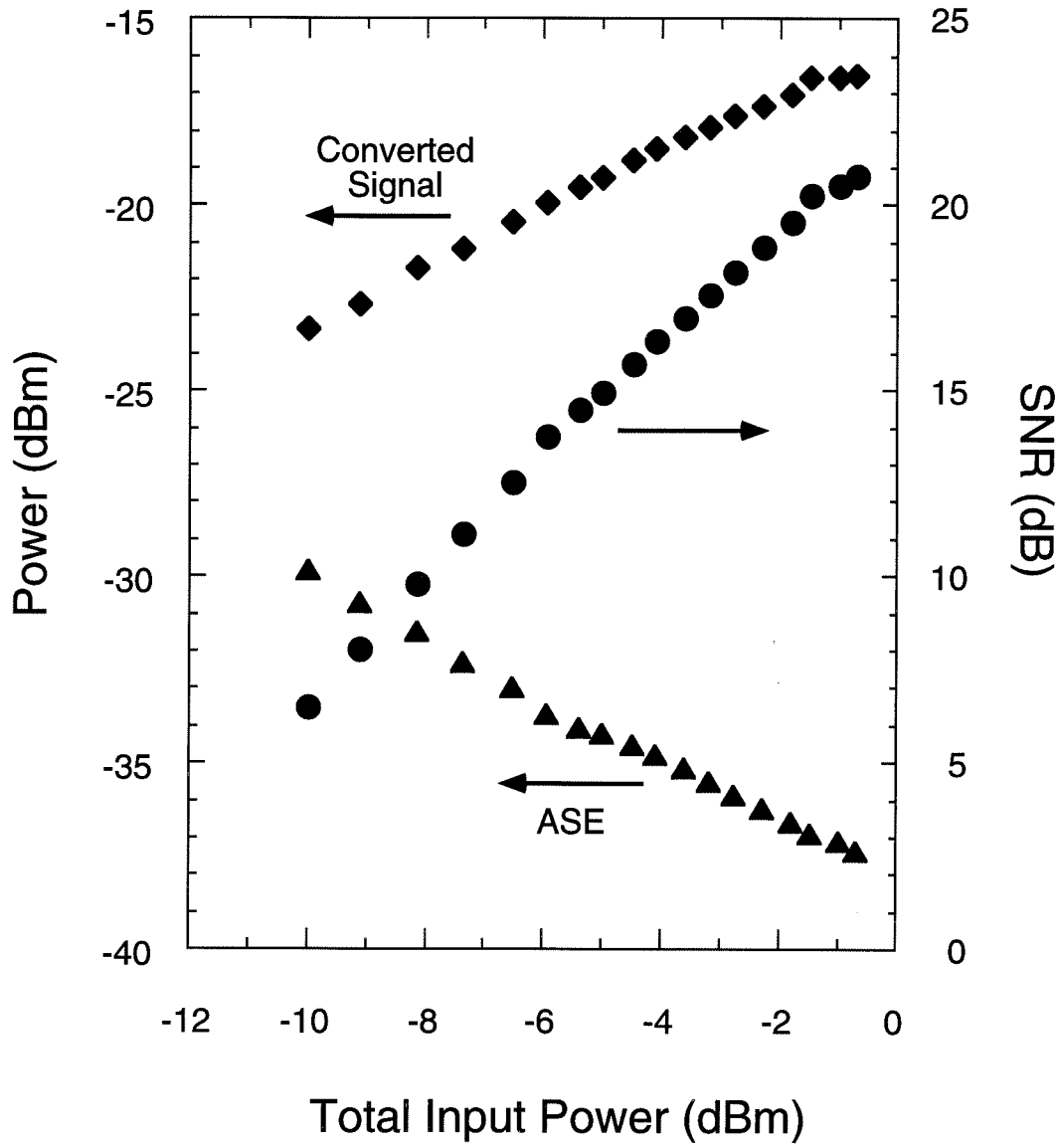

Figure 6.3: Measured four-wave mixing signal power, spontaneous noise (0.1 nm bandwidth), and optical SNR versus total input power. A tandem amplifier with two tensile strained SOA's was used.

equation derived from Eq. (6.1):

$$I^m_{out}(\nu_{cs}) = 3I^m_{out} + R(\Delta\lambda) + 10\log\frac{r}{(1+r)^3} \tag{6.7}$$

where $I^m_{out}(\nu_{cs})$ is the converted signal power in dBm, r is the ratio of amplified input signal to amplified pump and I^m_{out} (expressed in dBm) is the total output power, *i.e.*, the amplified pump power plus the amplified input power.

6.3.2 Noise Reduction

Spontaneous noise from the preamplification stage that resides in the conversion frequency band constitutes a major part of the noise at the converter's output, as indicated in Eq. (6.4). We refer to this component as the direct noise component. Unlike normal applications of optical preamplifiers in which amplification and spontaneous noise are inextricably connected, direct spontaneous noise associated with optical preamplification can, in principle, be eliminated, thereby vastly improving overall converter function. This can be done by introducing a filter between the preamplifier and the mixer which removes the preamplifier spontaneous noise component in the spectral vicinity of converted signal wavelength. This is possible since removal of noise components in the converted signal band at the mixer's input will have no effect on the subsequent mixing process. Such a filter which attenuates the converted signal bands by a factor of γ but leaves the input signal and pump bands unaffected will lead to a spontaneous noise reduction in dB given by

$$\text{Noise Reduction} = 10\log\frac{S^m_{in} + \frac{1}{2}F^m_n h\nu}{S^m_{in}/\gamma + \frac{1}{2}F^m_n h\nu} \tag{6.8}$$

where $F_n^m = 2n_{sp}^m\left(1 - \frac{1}{G_m}\right)$ is the SOA mixer's amplification noise figure. The converted input noise, which is normally much smaller than the amplified noise and the spontaneous noise introduced by the mixer, has been ignored in Eq. (6.8). It should be noted, however, that this converted noise would be the only remaining noise in an optimal converter scheme, as will be discussed later in this chapter.

Since the spontaneous noise introduced by the SOA mixer can be written as $\frac{1}{2}G_m F_n^m h\nu$, the term $\frac{1}{2}F_n^m h\nu$ can be viewed as the equivalent input noise power spectral density of the SOA mixer. The effectiveness of this noise reduction technique, as indicated in Eq. (6.8), strongly depends on the relative magnitude of the input noise power spectral density S_{in}^m coupled into the SOA mixer and the equivalent input noise power spectral density of the SOA mixer $\frac{1}{2}F_n^m h\nu$. The former, in turn, strongly depends on the excess noise of input signal and the preamplification gain, and the latter depends on the SOA mixer's noise as characterized by its amplification noise figure. Using $F_n^m = 8$ dB and $h\nu = 0.809$ eV, the calculated noise reduction is plotted in Figure 6.4 versus S_{in}^m for various filter extinction ratios γ.

We have experimentally verified this idea of noise reduction. A tunable erbium-doped fiber ring laser and a DFB laser were used as pump and input signal sources. The SOA mixer was the tensile strained InGaAs MQW amplifier [22] used in the spectroscopy study described in Chapter 4. An EDFA was used as the preamplifier for both the pump and input signal, followed by a fiber notch filter having 0.96 nm bandwidth, 14 dB extinction ratio centered at 1529.8 nm and near unity transmission outside of the filter band. The total optical power of the pump and input signal into

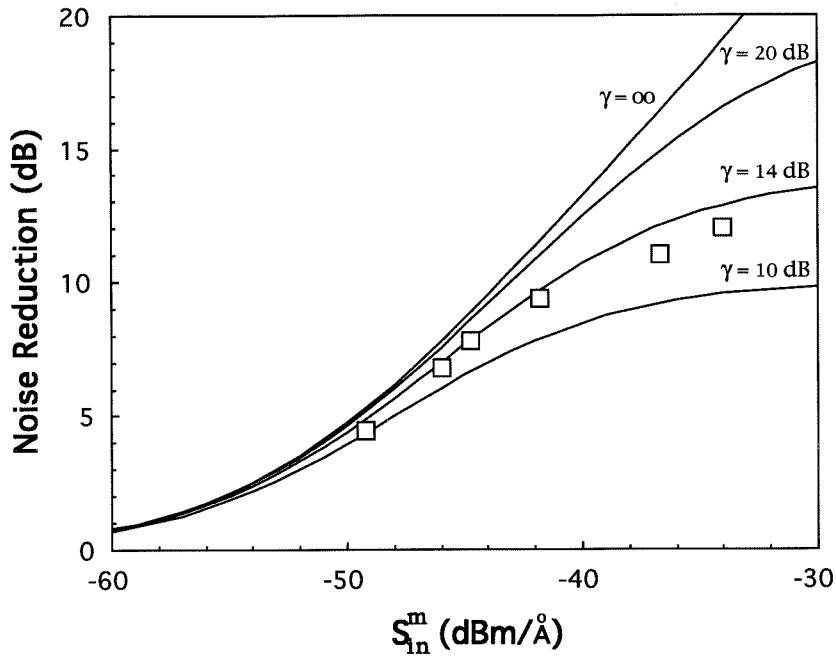

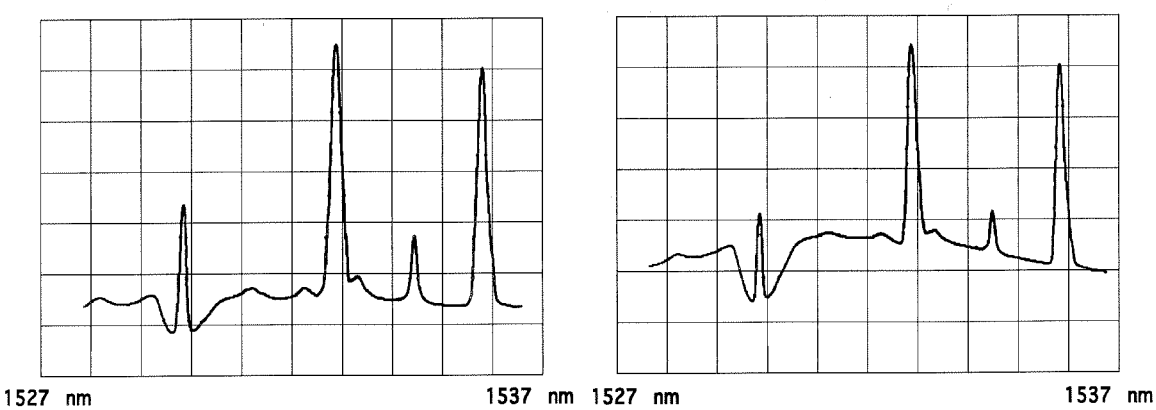

Figure 6.4: Upper figure shows noise reduction versus the spontaneous noise power density S_{in}^m at the SOA mixer's input; Lower picture illustrates the spectra of the SOA mixer's output for $S_{in}^m = -46.0$ dBm (left) and $S_{in}^m = -36.7$ dBm (right) showing spontaneous noise reduction. The small peak between the pump and input signal is a side mode of the DFB laser. Vertical scale: 10 dB/div; Horizontal scale: 1 nm/div.

the preamplifier was attenuated to vary the EDFA gain and thus the spontaneous noise power spectral density S_{in}^{m}. The measured noise reduction versus S_{in}^{m} is also presented in Figure 6.4 where a good agreement with theory can be seen. Also shown in Figure 6.4 are measured spectra of the SOA mixer's output where significant noise reduction is visible.

6.3.3 Optimal Converter Structure

The theoretical analysis and measurements described in this paper also suggest new considerations for optimal converter structures. Overall optical gain of the preamplifier and the SOA mixer has been previously shown to be crucial for high conversion efficiency. However, spontaneous noise introduced in the overall conversion process can considerably degrade the signal to noise ratio. To combat this problem, we propose to completely separate the functions of gain and nonlinearity.

In an optimal converter structure, the first stage would consist of two optical preamplifiers for the pump and input signal, respectively. Separate amplification of pump and input signal is advantageous because of better noise performance. Each of the preamplifiers is followed by a noise filter that removes spontaneous noise outside the pump band or input signal band. The third stage of the wavelength converter is the nonlinear mixer, which can be a highly saturated SOA, or a properly designed semiconductor waveguide with energy gap greater than the photon energy ($E_{gap} > h\nu$). In the former case the introduced spontaneous noise, as given by $n_{sp}^{m}(G_m - 1)h\nu$, depends on the SOA mixer saturation level, while in the latter case virtually no spontaneous noise is introduced by the mixer.

With this proposed structure, the high-gain preamplifiers provide high optical power into the mixer thereby maintaining efficient wavelength conversion in the mixer; however, they do not significantly contribute to the output spontaneous noise since filters can, in principle, eliminate the direct spontaneous noise in the converted signal band. Ideally, by using below gap mixing, only the converted spontaneous noise would remain in Eq (6.4). This would mean that signal to noise degradation would occur primarily in the preamplifiers, provided that the subsequent nonlinear wave mixing is efficient enough to ensure that, upon detection of the converted signal , the shot noise would not be a significant noise source. The mixing efficiency depends not only on the mixer's intrinsic parameters including the third order susceptibility and interaction length, but also on the preamplifier gain which determines powers of the pump and input signal at the mixer input. High gain preamplifiers are therefore also crucial to the noise performance of the overall conversion process.

6.4 Wavelength Conversion of Modulated Signal

We have characterized SOA four-wave mixing converters using a CW laser source as the input signal. These measurements have provided a good physical understanding of some of the most important converter characteristics such as conversion efficiency and noise properties. The understanding of these characteristics is essential to the design and optimization of these converters. In the meanwhile, we have begun to study four-wave mixing wavelength conversion from system's perspective. Wavelength conversion of 2.5 Gb/s and 10 Gb/s ASK data has been demonstrated and preliminary results

of this measurement are presented in this section.

A schematic diagram of the experimental setup used to demonstrate wavelength conversion of modulated signal is shown in Figure 6.5. The signal laser, a DFB laser operating at 1559.4 nm, was directly modulated at either 2.5 Gb/s or 10 Gb/s by a pseudorandom bit pattern of length $2^7 - 1$ supplied by a signal generator (Hewlett-Packard 70340A). The pump source was a tunable fiber-ring laser as shown in Figure 4.1, except here a tunable fiber-pigtailed interference bandpass filter with a bandwidth of about 1.5 nm was used in place of the broadband fiber Fabry-Perot filter. The outputs of the pump and signal lasers were combined using a 90/10 fiber-optic bidirectional coupler (pump 90%, signal 10%), and co-amplified in an Amoco EDFA with a maximum output power of 18 dBm. This preamplifier was followed by a fiber-grating notch filter having a 11.5 dB, 3 Å notch centered at 1551.5 nm. Although this converter structure was not quite the optimal structure that we proposed in the previous section, use of the notch filter, as we have discussed and will demonstrate, considerably reduced the excess noise from the preamplifier stage.

The SOA employed in the experiment was the tensile strained InGaAs MQW amplifier [22] used in the spectroscopy study described in Chapter 4. It was operated at a high injection current of 150 mA, but was strongly saturated by a total power of $\sim$ 13 dBm coupled into this SOA mixer using microscope objective lenses. The ratio of pump to input signal powers was maintained at about 10 dB, thereby ensuring that the slight modulation of the SOA gain by the input signal would not introduce waveform distortion and chirp to the converted signal.

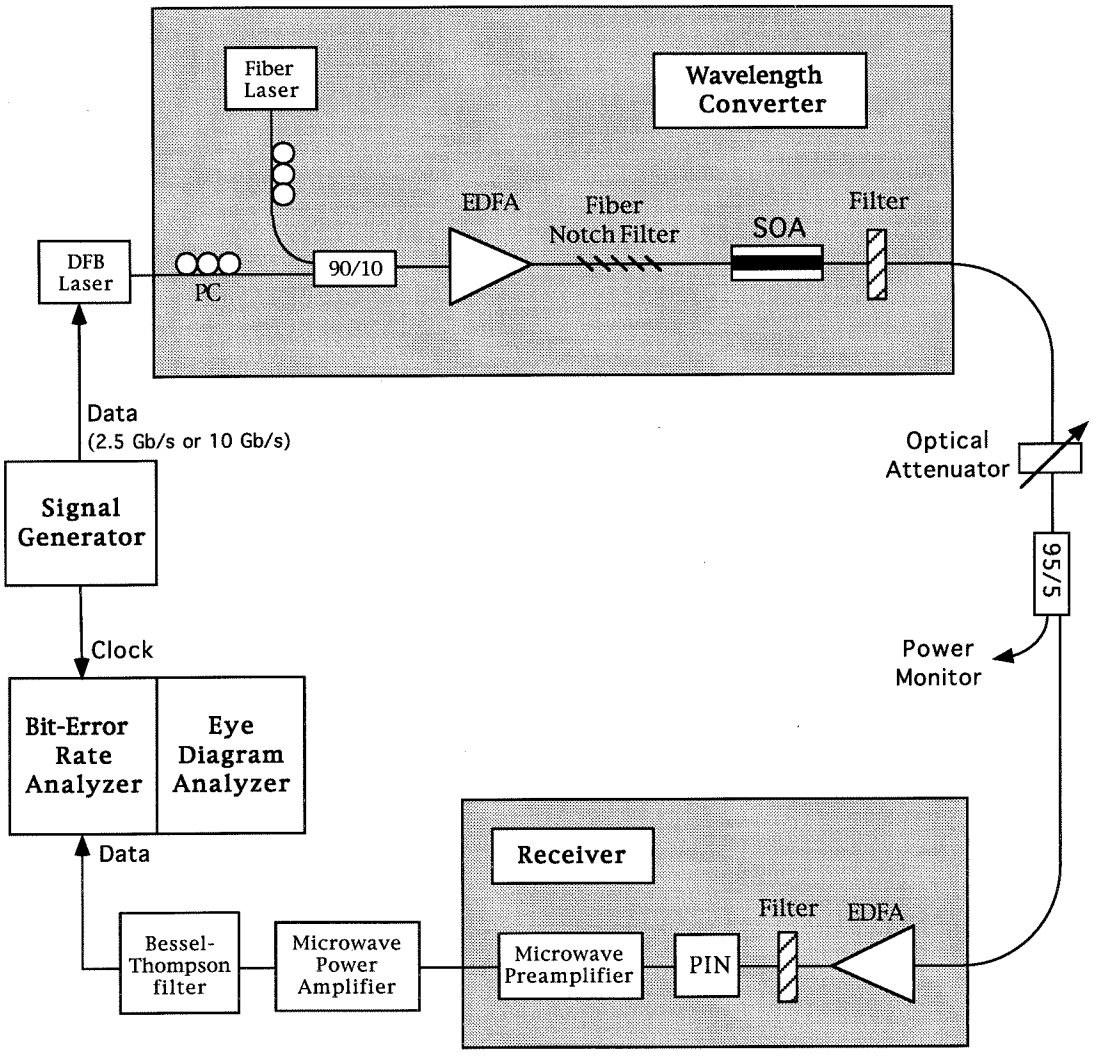

Figure 6.5: Experimental setup used to demonstrate wavelength conversion of ASK data at 2.5 Gb/s and 10 Gb/s.

By tuning the pump laser wavelength, the converted signal was set to the center of the notch filter. This corresponds to a wavelength down shift of 7.9 nm. The optical spectrum of the SOA output is shown in Figure 6.6(a) where the pump was slightly offset to illustrate the notch and the optical SNR improvement of the converted signal. A tunable fiber Fabry-Perot bandpass filter (bandwidth 35 GHz, finesse 100) was used to select the converted signal.

The converted signal was detected by a receiver consisting of an EDFA preamplifier, a *pin*-based lightwave converter with 15 GHz bandwidth (Hewlett-Packard 11982A), and a microwave preamplifier. A tunable fiber Fabry-Perot bandpass filter (bandwidth 45 GHz, finesse 100) was placed before the lightwave converter to remove most of the background spontaneous noise, also to further suppress residual pump, input signal. The detected data pattern was amplified by a microwave power amplifier (DC – 6 GHz) and analyzed either by a microwave transition analyzer (Hewlett-Packard 70820A) or by a BER tester (Hewlett-Packard 70843A). In the case of 2.5 Gb/s, a SONET OC-48 filter was used after the microwave amplifier to suppress high frequency noise.

A test waveform of the converted signal, consisting of repeated pattern 11100100 at 10 Gb/s, is shown in Figure 6.6(b). Typical eye diagrams for 2.5 Gb/s and 10 Gb/s are shown in Figures 6.6(c) and 6.6(d). These two eye diagrams correspond to BER's of approximately 1×10^{-9} and 1×10^{-7}, respectively. The greater amount of noise for 1 bits than for 0 bits, as seen from the measured waveform and the eye diagrams, indicates that the results were limited primarily by signal-spontaneous beat noise.

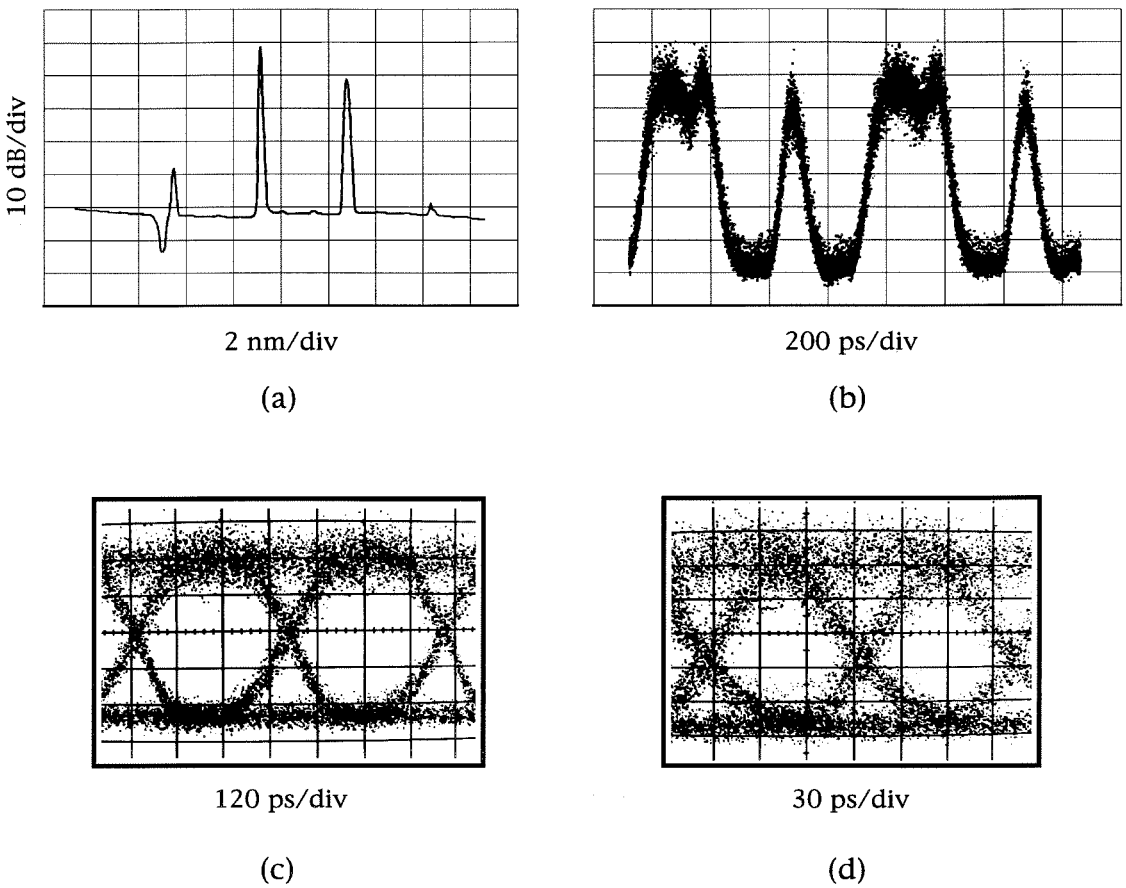

Figure 6.6: (a) Optical spectrum of SOA output; (b) converted data pattern 11100100; eye diagrams of converted data at (c) 2.5 Gb/s and (d) 10 Gb/s.

The in-fiber converted signal power in this study was measured to be $-26 \sim -28$ dBm and the optical SNR was $26 \sim 28$ dB (bandwidth 0.1 nm). These optical parameter would give error-free performance at 10 Gb/s with a high-performance optically-preamplified receiver. In fact, the optical spectra measured at the EDFA preamplifier's input and output show that the amplified spontaneous noise introduced by the preamplifier, rather than the amplified input excess noise, was the dominant source of noise at the *pin* detector. This indicates that the optical preamplifier was the primary limiting factor in this measurement.

6.5 Conclusion

We have characterized some of the most important converter characteristics such as conversion efficiency and noise properties. We have also demonstrated wavelength conversion of modulated signals at data rates of 2.5 Gb/s and 10 Gb/s. Due to the lack of a high-performance EDFA preamplifier and a sufficiently stable tunable pump source in this preliminary system measurement, we did not perform measurements of BER versus received power. Improvement to the receiver's optical preamplifier, however, is expected to enable a full characterization of the impact of the SOA four-wave mixing wavelength converters on fiber-optic communication systems. In addition, overall optimization of the wavelength converter structure should lead to further improvement to the converter performance.

Bibliography

[1] C. K. Kao and G. A. Hockham, "Dielectric-fiber surface waveguides for optical frequency," *IEE Proc.* vol. 113, pp. 1151–1158, 1966.

[2] F. P. Kapron, D. B. Keck, and R. D. Maurer, "Radiation losses in glass optical waveguides," *Appl. Phys. Lett.*, vol. 17, pp. 432–434, 1970.

[3] I. Hayashi, M. B. Panish, P. W. Foy, and S. Sumski, "Junction lasers which operate continuously at room temperature," *Appl. Phys. Lett.*, vol. 17, pp. 109–111, 1970.

[4] S. E. Miller and I. P. Kaminow, Eds., *Optical Fiber Telecommunications II*, Academic Press, 1988.

[5] G. P. Agrawal, *Fiber-Optic Communication Systems*, John Wiley & Sons, 1992.

[6] T. Li, "The impact of optical amplifiers on long-distance lightwave telecommunications," *Proc. IEEE*, vol. 81, pp. 1633–1646, 1993.

[7] A. R. Chraplyvy, J. M. Delavaux, R. M. Derosier, G. A. Ferguson, D. A. Fishman, C. R. Giles, J. A. Nagel, B. M. Nyman, and J. W. Sulhoff, "1420 km transmission of 16 2.5 Gb/s channels using silica-fiber-based EDFA repeaters," *IEEE Photon. Technol. Lett.*, vol. 6, pp. 1371–1373, 1994.

[8] A. R. Chraplyvy, A. H. Gnauck, R. W. Tkach, R. M. Derosier, C. R. Giles, B. M. Nyman, G. A. Ferguson, J. W. Sulhoff, and J. L. Zyskind, "One-third Terabit/s transmission through 150 km of dispersion-managed fiber," *IEEE Photon. Technol. Lett.*, vol. 7, pp. 98–100, 1995.

[9] S. B. Alexander *et al.*, "A precompetitive consortium on wide-band all-optical networks," *IEEE J. Lightwave Technol.*, vol. 11, pp. 714–735, 1993.

[10] C. A. Brackett, A. S. Acampora, J. Sweitzer, G. Tangonan, M. T. Smith, W. Lennon, K-C Wang, and R. H. Hobbs, "A scalable multiwavelength multihop optical network: a proposal for research on all-optical networks," *IEEE J. Lightwave Technol.*, vol. 11, pp. 736–753, 1993.

[11] H. Kawaguchi, K. Magari, H. Yasaka, M. Fukada, and K. Oe, "Tunable optical-wavelength conversion using an optically triggerable multi-electrode distributed feedback laser diode," *IEEE J. Quantum Electron.*, vol. 24, pp. 2153–2159, 1988.

[12] J. M. Wiesenfeld, B. Glance, J. S. Perino, and A. H. Gnauck, "Wavelength conversion at 10 Gb/s using a semiconductor optical amplifier," *IEEE Photon. Technol. Lett.*, vol. 5, pp. 1300–1303, 1993.

[13] T. Durhuus, R. J. S. Pedersen, B. Mikkelsen, K. E. Stubkjaer, M. Öberg, and S. Nilsson, "Optical wavelength conversion over 18 nm at 2.5 Gb/s by DBR-laser," *IEEE Photon. Technol. Lett.*, vol. 5, pp. 86–88, 1993.

[14] C. Q. Xu, H. Okayama, K. Shinozaki, K. Watanabe, and M. Karahara, "1.5 μm band efficient broadband wavelength conversion by difference frequency generation in a periodically domain-inverted $LiNbO_3$ channel waveguide," *Appl. Phys. Lett.*, vol. 63, pp. 3559–3561, 1993.

[15] K. Inoue and H. Toba, "Wavelength conversion experiment using fiber four-wave mixing," *IEEE Photon. Technol. Lett.*, vol. 4, pp. 69–72, 1992.

[16] S. Murata, A. Tomita, J. Shimizu, and A. Suzuki, "THz optical frequency conversion of 1 Gb/s signal using highly nondegenerate four-wave mixing in an InGaAsP semiconductor laser," *IEEE Photon. Technol. Lett.*, vol. 3, pp. 1021–1023, 1991.

[17] M. C. Tatham, G. Sherlock, and L. D. Westbrook, "20 nm wavelength conversion using nondegenerate four-wave mixing," *IEEE Photon. Technol. Lett.*, vol. 5, pp. 1303–1306, 1993.

[18] J. Zhou, N. Park, J. W. Dawson, K. J. Vahala, M. A. Newkirk, and B. I. Miller, "Efficiency of broadband four-wave mixing wavelength conversion using semiconductor traveling-wave amplifiers," *IEEE Photon. Technol. Lett.*, vol. 6, 50–52, 1994.

[19] R. Ludwig and G. Raybon, "BER measurements of frequency converted signals using four-wave mixing in a semiconductor laser amplifier at 1, 2.5, 5 and 10 Gbit/s," *Electron. Lett.*, vol. 30, pp. 338–339, 1994.

[20] J. Zhou, N. Park, K. J. Vahala, M. A. Newkirk, and B. I. Miller, "Broadband wavelength conversion with amplification by four-wave mixing in semiconductor traveling-wave amplifiers," *Electron. Lett.*, vol. 30, pp. 859–860, 1994.

[21] J. Zhou and K. J. Vahala, "Spontaneous noise reduction in four-wave mixing wavelength converters," *Conference on Lasers and Electro-Optics*, Baltimore, Maryland, May 21–26, 1995, paper CThT1.

[22] B. I. Miller, U. Koren, M. A. Newkirk, M. G. Young, R. M. Jopson, R. M. Derosier and M. D. Chien, "Tensile-strained InGaAs/InGaAsP quantum-well optical amplifier with a wide spectral gain region at 1.55 μm," *IEEE Photon. Technol. Lett.*, vol. 5, pp. 520–522, 1993.